Geochemical characterisation of the Danish subsurface ash series for carbon mineralisation potential

ANNA BUHL PEDERSEN, NIELS HEMMINGSEN SCHOVBO, STÉPHANE BODIN, ARKA RUDRA, DAVID LUNDBEK EGHOLM, OLE RØNØ CLAUSEN, CHRISTIAN TEGNER & HAMED SANEI

Geological Society of Denmark
https://2dgf.dk

Received 30 May 2025
Accepted in revised form 7 October 2025
Published online 05 November 2025

Buhl Pedersen, A., Schovsbo, N.H., Bodin, S., Rudra, A., Egholm, D.L., Clausen, O.R., Tegner, C. & Sanei, H. 2025. Geochemical characterisation of the Danish subsurface ash series for carbon mineralisation potential. Bulletin of the Geological Society of Denmark, Vol. 74, pp. 227–250. ISSN 2245-7070. https://doi.org/10.37570/bgsd-2025-74-13

The Danish subsurface ash series within the Eocene-aged Fur and Ølst Formations has a large theoretical CO_2 storage capacity through carbon mineralisation, a potential that is the main motivation behind the C·ASH project initiated by researchers from the Department of Geoscience, Aarhus University. The potential carbon storage is achieved by injection of CO_2 into the closely spaced volcanic ash beds in the Danish subsurface to accelerate silicate dissolution, leading to carbon fixation by mineralisation of CO_2 as carbonate minerals. This provides a valuable alternative to conventional CO_2 storage technologies that typically aim to store CO_2 as a supercritical phase in deep porous aquifers. One of the essential requirements for the mineralisation technology is the identification of ash beds that contain enough reactive divalent cations (Ca^{2+}, Fe^{2+}, Mg^{2+}) to sustain the silicate dissolution – carbonate precipitation reactions. This study aims to provide a geochemical proxy to identify and locate suitable ash beds with high CO_2 sequestration potential. For this purpose, the shallow Harre borehole drilled in 1980 in northwestern Denmark is analysed using high-resolution XRF and SEM-EDS. In the Harre well the ash beds are most abundant within a five meters thick interval in the uppermost part of the Ølst Formation between 191 and 196 meters below surface. The XRF data show that titanium (Ti) is the most reliable elemental proxy for identifying the volcanic ash beds and that calcium (Ca), which is an important divalent cation for carbon mineralisation, is mostly enriched in the volcanic ash beds within the five meters interval. However, Ca may also be associated with gypsum ($CaSO_4 \cdot 2H_2O$) and carbonates ($CaCO_3$), suggesting that part of the Ca have already leached from silicates within the ash beds. This fraction is believed to be low and that the ash beds' suitability for carbon mineralisation remain high.

Keywords: Carbon mineralisation, volcanic ash, geochemical proxy, XRF, SEM-EDS.

Anna Buhl Pedersen [abp@geo.au.dk], Department of Geoscience, Aarhus University, Høegh-Guldbergs Gade 2, DK-8000 Aarhus C, Denmark. Niels Hemmingsen Schovbo [nsc@geus.dk], Geological Survey of Denmark and Greenland (GEUS), Øster Voldgade 10, DK-1350 Copenhagen K, Denmark. Stéphane Bodin [stephane.bodin@geo.au.dk], Arka Rudra [arudra@geo.au.dk], David Lundbek Egholm [egholm@geo.au.dk], Ole Rønø Clausen [ole.r.clausen@geo.au.dk] and Hamed Sanei [sanei.geo.au.dk], Department of Geoscience, Aarhus University, Høegh-Guldbergs Gade 2, DK-8000 Aarhus C, Denmark.

Promising mechanisms for Carbon Capture and Storage (CCS) has been known for many decades and play a vital role in the continuous efforts to achieve net zero CO_2 emissions (IPCC 2005). Conventional carbon storage, where supercritical CO_2 is injected into deep, permeable geological reservoirs sealed by an impermeable caprock, is considered important in managing the effects of climate change (Baklid *et al.* 1996; Torp & Gale 2004; IPCC 2005, 2018, 2023). However, other alternatives are needed to diversify the possibility of carbon storage. One such alternative is carbon mineralisation through silicate dissolution, where carbon is stored permanently as carbonate minerals by accelerating the natural process of the carbon-silicate cycle (Seifritz 1990; Lackner *et al.* 1995; Snæbjörnsdóttir *et al.* 2020). By injecting aqueous-dissolved or liquid CO_2 into reactive rocks like basalts, divalent cations are leached out through silicate dissolution, which eventually results in the precipitation of carbonate minerals (Eq. 1–2).

$$(Ca, Mg, Fe)SiO_{3(s)} + 2\,CO_{2(g)} + H_2O_{(l)} \rightleftharpoons (Ca, Mg, Fe)^{2+}_{(aq)} + 2\,HCO^{-}_{3(aq)} + SiO_{2(aq)} \quad (1)$$

$$(Ca, Mg, Fe)^{2+}_{(aq)} + 2\,HCO^{-}_{3(aq)} \rightleftharpoons (Ca, Mg, Fe)CO_{3(s)} + CO_{2(g)} + H_2O_{(l)} \quad (2)$$

As an addition to a more permanent way to store CO_2, mineralisation through silicate dissolution significantly reduces the time it takes for CO_2 to be mineralised, which is no more than a few years (Snæbjörnsdóttir *et al.* 2017). The process has been successfully demonstrated in Iceland through the CarbFix project, which since 2012 continues to store CO_2 in a basaltic subsurface (Aradóttir *et al.* 2011; Gíslason *et al.* 2018; Snæbjörnsdóttir *et al.* 2020). The Carbfix injection site at Hellisheiði is ideal for carbon mineralisation due to the basaltic subsurface together with a well-documented hydrothermal system providing the optimal permeability and temperature to quickly mineralise the CO_2 (Snæbjörnsdóttir *et al.* 2020). A basalt-rich geology of this character and setting is, however, not accessible everywhere in the world and to maximise the potential utilisation of carbon mineralisation globally, further research is needed to identify suitable rock types in the subsurface with similar reactive character.

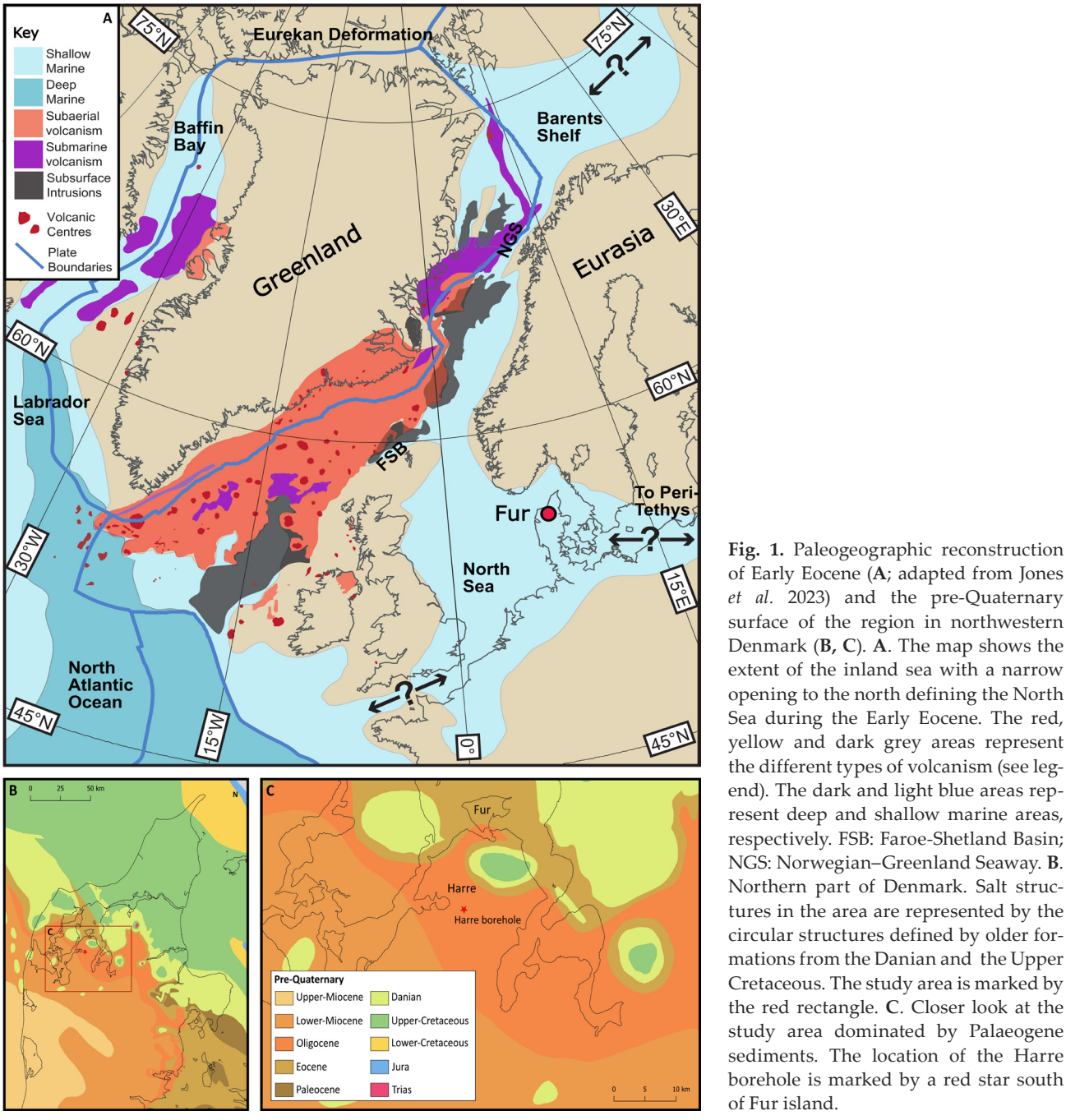

Fig. 1. Paleogeographic reconstruction of Early Eocene (**A**; adapted from Jones *et al.* 2023) and the pre-Quaternary surface of the region in northwestern Denmark (**B, C**). **A**. The map shows the extent of the inland sea with a narrow opening to the north defining the North Sea during the Early Eocene. The red, yellow and dark grey areas represent the different types of volcanism (see legend). The dark and light blue areas represent deep and shallow marine areas, respectively. FSB: Faroe-Shetland Basin; NGS: Norwegian–Greenland Seaway. **B**. Northern part of Denmark. Salt structures in the area are represented by the circular structures defined by older formations from the Danian and the Upper Cretaceous. The study area is marked by the red rectangle. **C**. Closer look at the study area dominated by Palaeogene sediments. The location of the Harre borehole is marked by a red star south of Fur island.

During the Late Paleocene/Early Eocene, more than 180 volcanic ash beds with a basaltic to rhyolitic composition (Larsen *et al.* 2003) were deposited in the North Sea area in connection with the opening of the Atlantic Ocean and creation of the North Atlantic Igneous Province (NAIP; Knox *et al.* 2010; Stokke *et al.* 2020, 2021). In the northwestern part of Denmark, ash beds are found in the Fur and Ølst formations (Bøggild 1918; Pedersen 1981; Pedersen & Surlyk 1983, Heilmann-Clausen 1995). Farther south in Denmark, the volcanic ash beds are found 200–300 m below the surface (Nielsen *et al.* 1994). The majority of the ash has a composition akin to the basalts in Iceland and exhibit primary textures including glassy fragments (Larsen *et al.* 2003) and thus has the potential to store large amounts of CO_2 via the carbon mineralisation process. This concept is the main idea behind the C·ASH project (Carbon Fixing by Volcanic Ash) initiated by researchers from the Department of Geoscience, Aarhus University and Climate Foundation Skive (Climate Foundation Skive 2025).

The aim of this study is to explore and analyse the whole-rock geochemistry of the Danish subsurface Ash Series present in the Harre drill core obtained in 1980 (GEUS 1980; Nielsen *et al.* 1994; Heilmann-Clausen 1995). By using high-resolution X-Ray fluorescence (XRF) analyses and Scanning Electron Microscopy – Energy Dispersive X-ray Spectrometry (SEM-EDS), new geochemical proxies can be used in combination with conventional lithological description to quickly recognize the presence of the Danish subsurface Ash Series in future boreholes. In the case of carbon mineralisation, potential target zones as well as zones of geochemical and lithological importance can also be distinguished.

Geological setting

During the Early Eocene, the Danish area and the rest of the North Sea Basin were covered by an inland sea, which for a brief period of 1 million years only had a connection to open water through the narrow Norwegian–Greenland Sea (Fig. 1A; Knox *et al.* 2010). During that time, deposition of thick packages of shales and mudstones dominated in the Danish area (Dinesen *et al.* 1977; Nielsen *et al.* 1986; Heilmann-Clausen 1995; Pedersen *et al.* 2011). In conjunction to the volcanic activity as well as the early rifting of the North Atlantic Ocean, volcanic ash beds spread widely over the region and can be tracked as far away from the NAIP as Austria (Andersen 1937; Larsen *et al*. 1999; Egger *et al.* 2000). These ash beds define Sequence 1.2 of the Danish area and contain the Fur and Ølst formations (Heilmann-Clausen *et al.* 1985; Michelsen *et al.* 1999). They constitute excellent stratigraphical markers to correlate the sediments of the North Sea and means to estimate the volume and frequency of different stages of volcanism associated with the rifting and creation of NAIP (Pedersen 1981; Pedersen & Surlyk 1983; Morton & Evans 1988; Schmitz & Asaro 1996; Larsen *et al*. 2003; Jones *et al.* 2019; Stokke *et al.* 2020; Stokke *et al.* 2021; Jones *et al.* 2023).

In most of the North Sea and onshore Denmark, the volcanic ash beds are situated in mudstones and clay formations known as Balder and Sele formations in the central North Sea and the Ølst Formation onshore (Heilmann-Clausen *et al.* 1985; Nielsen *et al.* 1986; Danielsen & Thomsen 1997; Schiøler *et al*. 2007). However, in the northwestern part of Denmark the ash beds can be found interbedded with diatomite, locally known as 'Moler', defining the Fur Formation (Pedersen & Surlyk 1983). This diatomite interval can be tracked along a narrow belt stretching northwest along the Norwegian coast, believed to represent a narrow upwelling zone driven by northern winds (Bonde 1973, 1974, 1979; Thomsen & Danielsen 1995; Danielsen & Thomsen 1997). The upwelling would cause the bottom waters to become poor in oxygen, reflected by well-laminated diatomite (Pedersen 1981; Pedersen & Surlyk 1983).

The Harre borehole

In May 1980, the drilling of the Harre borehole was completed. The borehole is located close to the village of Harre located south of the island of Fur (Fig. 1B, C). During the drilling, core sections in plastic core liners of 1.5 m in length and 10 cm in diameter were retrieved (GEUS 1980; Nielsen 1994a). The present part of the ash layers in the Harre borehole is recognized from 190.88–222.00 meters below surface (m b.s.), with a total thickness of 31.12 m. The facies of the Fur and Ølst formations interfinger in a characteristic way, where the diatomitic Fur Formation is interbedded between an upper and lower clay interval belonging to the Ølst Formation with gradual transitions (Fig. 2). The interfingering stratigraphy contrasts with most of the Danish area, where the two formations are geographically separated (Heilmann-Clausen *et al.* 1985; Nielsen 1994b). More importantly, the majority of the ash beds in the borehole occurs in the upper clay interval of the Ølst Formation. These ash beds mainly represent the positive series in the Ash Series as established by Bøggild (1918) and Gry (1940). From the Harre core sections, strata are missing from the transition from Fur Formation to the upper part of the Ølst Formation and at the transition between the lower part of the Ølst Formation and Holmehus Formation (Nielsen *et al.* 1994; Nielsen 1994b).

The upper part of the Ølst Formation is present

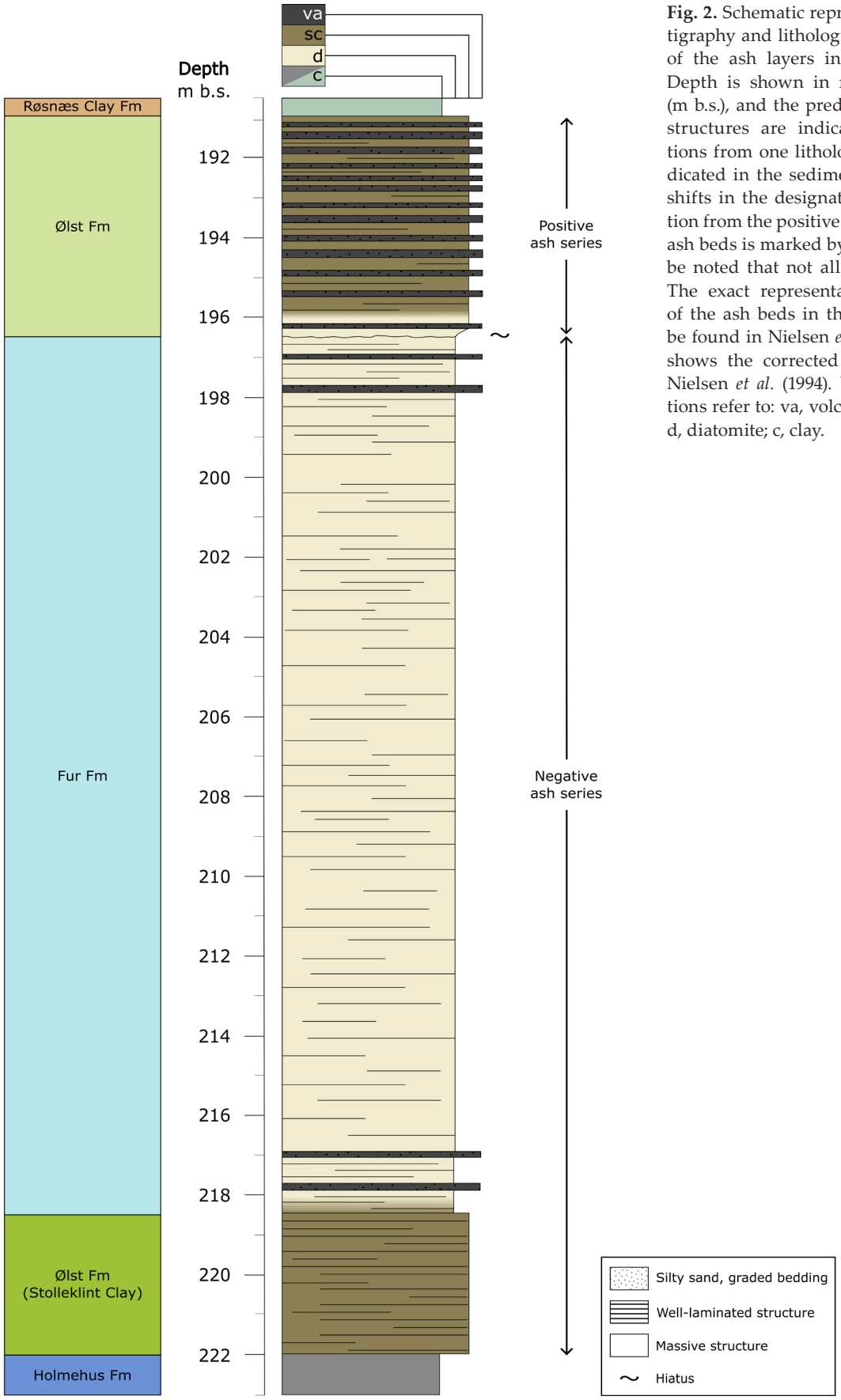

Fig. 2. Schematic representation of the stratigraphy and lithologies of the present part of the ash layers in the Harre borehole. Depth is shown in meters below surface (m b.s.), and the predominant sedimentary structures are indicated. Gradual transitions from one lithology to another are indicated in the sedimentary log by gradual shifts in the designated colors. The transition from the positive to negative numbered ash beds is marked by the arrows. It should be noted that not all ash beds are shown. The exact representation and numbering of the ash beds in the Harre borehole can be found in Nielsen *et al.* (1994). The figure shows the corrected depths according to Nielsen *et al.* (1994). Lithological abbreviations refer to: va, volcanic ash; sc, silty clay; d, diatomite; c, clay.

from 190.88–196.5 m b.s. in the Harre borehole and consists of non-diatomaceous, greenish grey clay. At the bottom of the interval, the clay gradually becomes less dense and appears similar to the underlying diatomite. The volcanic ash beds vary between black and dark grey in color with a sandy silt grain size (Nielsen 1994b; Nielsen *et al*. 1994). Occasionally, burrows and signs of reworked material are present (Nielsen *et al*. 1994). Based on grain size analyses, the sand content increases in the upper part of the Ølst Formation, likely caused by mixing of the ash beds and silt due to bioturbation (Nielsen 1994b). The following interval (196.5–218.5 m b.s.) is recognized as the diatomite belonging to the Fur Formation. Within the Fur Formation, three different types of clay have been distinguished based on changes in lamination from well-laminated to poorly laminated or massive structures. The positions of the three types of clay within the Fur Formation show complex and interfingering relations due to fluctuations in the diatom/clay ratio (Nielsen *et al*. 1994). The Fur Formation contains a few ash beds widely spaced from each other, which contrasts with the overlying Ølst Formation. The ash beds in the present part of the Fur Formation in the Harre borehole mostly belong to the negative series of the ash bed stratigraphy of Bøggild (1918) and Gry (1940). The lowest clay interval (218.5–222 m b.s.) belongs to the Stolleklint Clay of the Ølst Formation and consists of non-diatomaceous clay, similar to the clay in the upper part of the Ølst Formation. It contains few thin ash beds. In contrast to the upper clay interval in the Ølst Formation, lamination is present (Nielsen *et al.* 1994).

Material, methods and data analysis

The methods used in this study consist of handheld X-ray fluorescence (HH-XRF) measurements, Scanning Electron Microscopy - Energy Dispersive X-ray Spectrometry (SEM-EDS), micro-X-ray fluorescence spectrometry (μ-XRF) and pyrolysis, as well as a range of data analysis such as normalisation and multivariate statistical analysis. The measurements and analyses were conducted at the Department of Geoscience and at the Interdisciplinary Nanoscience Centre (iNANO) at Aarhus University. From the Harre drill core, nineteen core sections approximately 1.5 m long each were selected. The core sections numbered 128–148 constitute the interval of 190.5 to 222.0 m b.s. in the borehole. The core sections were chosen to include the ash beds of the Ash Series in the units corresponding to the Ølst and Fur formations. Core sections 141 and 144 (depth intervals 210.0–211.5 and 214.5–216.0 m b.s.) were not available for analysis.

Handheld (HH) XRF analysis

A Bruker SI TITAN handheld XRF device was used to establish elemental variation. The depth of penetration is around 1 cm with a spot size of ~8 mm. The procedure was as follows: the plastic core liners were opened with a saw and the surface was scraped clean of drill mud to provide a clean, relatively flat surface. Each sample was analysed for 60 seconds for every cm as continuously along the cores as possible.

For every core section, three standard measurements were performed before and after the measurements on the core. Furthermore, the standard was measured for every sixth measurement in average to control the stability of the instrument. The standard used was the CS-M2 GEO/SOIL sample available at the Department of Geoscience. Reproducibility of the standard measurements revealed precision to be better than 10% for most of the analysed elements with the exceptions of S (33%) and P (17%; Table 1). Standard averages were only available for a selection of elements, and accuracy calculations were therefore limited. However, for the available averages, accuracies remain better than 10% except for K regarding the concentrations of the standard (Table 1).

Quality of the Harre drill core

Ideally, the geochemical variations in a sediment core would be obtained using an XRF core scanner. The reason for using a HH-XRF instrument for this study

Table 1. Descriptive statistics of HH XRF standard measurements

Element	Al	Si	P	S	K	Ca	Ti	Mn	Fe	Ni	Cu	Zn	As	Sr	Zr	Pb
Mean	6.283	32.160	0.034	0.171	3.763	0.662	0.153	0.096	1.651	0.004	0.020	0.073	0.007	0.016	0.023	0.086
Median	6.352	32.471	0.033	0.161	3.789	0.663	0.152	0.097	1.654	0.004	0.020	0.073	0.007	0.016	0.023	0.086
St.dev.	0.542	1.896	0.006	0.056	0.290	0.046	0.009	0.009	0.125	0.001	0.002	0.005	0.001	0.001	0.001	0.003
Max	7.399	35.826	0.052	0.440	4.446	0.770	0.178	0.124	1.920	0.006	0.024	0.085	0.010	0.018	0.027	0.094
Min	3.791	22.233	0.011	0.070	2.842	0.499	0.121	0.068	1.269	0.002	0.015	0.057	0.003	0.014	0.020	0.077
n	266	266	266	266	266	266	266	266	266	266	266	266	266	266	266	86
Precision (%)	8.6	5.9	16.9	32.5	7.7	7.0	6.0	9.3	7.5	16.1	8.1	6.2	19.0	3.7	4.6	3.8
Accuracy (%)	9.0	7.2	–	–	12.3	–	–	1.7	2.9	6.6	1.0	–	–	–	–	3.0
MOE	0.077	0.271	0.001	0.008	0.041	0.007	0.001	0.001	0.018	0.000	0.000	0.001	0.000	0.000	0.000	0.001
Standard (average)	6.900	34.660	–	–	4.292	–	–	0.098	1.700	0.004	0.020	–	–	–	–	0.083

is based on the overall state of the core sections. The cores had dried out and are intensively fractured, posing challenges to measure continuously along the sections. The core had not been halved either, which meant that a flat measurement surface was not readily available for the analysis. Samples from previous studies of the core were occasionally present in small plastic bags. In some intervals the volcanic ash beds were completely unconsolidated and mixed with pieces of clay and diatomite, which made it challenging to provide a representable result for the ash beds in question. It is, however, not uncommon for deep drill cores to be in a similar condition. An available drill core is still far more superior to well cuttings and outcrops in terms of coherent stratigraphy and determination of details such as formation boundaries and sedimentary structures. Regarding the geochemical variations and sampling it also provides a more accurate estimation, as e.g. well cuttings can be compromised by drilling mud contamination and alteration (Sanei *et al*. 2020). A HH-XRF instrument was therefore considered the most suitable approach, as the measurable surfaces can be determined manually. Furthermore, the XRF data obtained in this study have successfully reflected the lithologies in the Harre drill core as established by Nielsen *et al.* (1994), revealing distinct trends related to the volcanic ash as well as the diatomite. The trends will be discussed in the following.

Centred log ratio (clr) transformation and Principal Component Analysis (PCA)

Since this study deals with compositional data, normalisation is needed before multivariate statistical analyses can be performed on the data to eliminate any spurious relationships between the components (Aitchison 1984). Centred log ratio (clr) transformation is commonly used on geochemical data and is therefore used for the normalisation of the HH-XRF data. The clr transformation normalises the data by taking the natural logarithm of the ratio of each data value divided by the geometric mean of all parts of the analysis point. In this way misinterpretations can be avoided during further statistical analysis of the data. To use the clr transformation, false zeros such as values measured below detection limit need to be handled. Therefore, the corresponding standard error value divided by two was used (Schovsbo & Petersen 2024). Variables that are dominated by measurements below detection limit are deemed unsuitable and excluded from the dataset before normalisation and further analysis. Of the elements and oxides deemed suitable for analysis, 15.3% of the data consist of measurements below detection limit (supplementary file A). The clr normalised data have further been auto-scaled and centred.

To identify any hidden patterns or correlations within the clr normalised XRF data, Principal Component Analysis (PCA) was used. PCA is a widely used statistical tool to reduce high-dimensional geochemical data into linearly uncorrelated variables called principal components; a set of vectors that explain the variance in the dataset. By reducing the high-dimensional dataset, it is possible to visualise the data in a two-dimensional space (Kherif & Latypova 2020). The data matrix of the HH-XRF data defines the elements and oxides as variables and the depth point compositional values as observations. This is used to analyse correlations between the occurrences of the elements and oxides with regards to the different lithologies and secondary deposits present.

Table 2. Samples analysed with SEM-EDS, μ-XRF and pyrolysis

Sample ID	Sample depth (m b.s.) uncorrected	Lithology
HA-2	191.12	Volcanic ash (+118)
HA-1	191.27	Clay layer (upper clay interval)
HA-3	192.90	Volcanic ash (+90D)
HA-7	196.79	Diatomite
HA-5	207.82	Diatomite
HA-6	208.98	Diatomite
HA-4	220.24	Clay layer (lower clay interval)

+118 and +90D refer to the respective volcanic ash beds from which the samples were taken. Depths are uncorrected according to Nielsen *et al.* (1994).

Scanning Electron Microscopy – Energy Dispersive X-ray Spectrometry (SEM-EDS)

Based on the HH-XRF measurements, seven samples were chosen at different depths in different lithologies for further analysis using SEM-EDS (Table 2). To mount the samples on the sample stubs, a conducting carbon cement (Leit-C) was used. Before performing SEM-EDS, the samples were coated with platinum (Pt) using the LEICA EM SCD 500 sputter coater. The mounting and coating were performed at iNANO, Aarhus University. For SEM-EDS, the TESCAN VEGA scanning electron microscope sourced by tungsten filament electrons and with integrated EDS was used; it is housed at the Department of Geoscience, Aarhus University. The used accelerator voltage was set to 15 kV. The SEM images were obtained using the TESCAN Essence™ software and the elemental analysis of the chosen samples were obtained using the Aztec software from Oxford Instruments.

Pyrolysis analysis

Pyrolysis analysis was performed using a HAWK Pyrolyser and Total Organic Carbon (TOC) analyser

(Wildcat Technologies, U.S.A.). Approximately 50 mg of sample was initially purged to 300 °C (resulting in the S0 peak), then pyrolysed at 300 °C for 3 minutes, producing the S1 peak, which represents free hydrocarbons (HC). Following this, a temperature ramp of 25 °C/min was applied up to 650 °C, during which hydrocarbons (S2 peak), CO (S3 CO peak), and CO_2 (S3 CO_2 peak) were continuously measured. These measurements correspond to the labile organic carbon. In this study, the value of S1 (free HC) is considered as the sum of S0 + S1 (expressed in mg HC/g rock; Rudra *et al.* 2024). After the pyrolysis phase, the sample was purged under an oxygen atmosphere and reheated from 150 °C to 850 °C (25 °C/min). The CO and CO_2 released during this step represent the residual carbon fraction (Lafargue *et al.* 1998) until 700 °C, beyond which the CO_2 released is calculated as mineral carbon. The total organic carbon (TOC) content is the sum of the labile (reactive) and residual (inert) organic carbon (see supplementary file A).

Micro-X-ray Fluorescence Spectrometry (μ-XRF)

Seven samples used for SEM-EDS were further analysed using μ-XRF. The purpose of using μ-XRF was to support and semi-quantify the findings of the SEM-EDS analysis as well as to determine the geochemical compositions and distribution of elements in the samples. For this purpose, area scans were obtained, where average element and oxide quantifications of the samples were measured (supplementary file B). The μ-XRF data is produced based on a standardless quantification using the M-Quant software provided by the instrument. Based on earlier studies, the quantification of the elements and oxides wt.% have shown good long-term consistency and reliability of instrument performance (Birch *et al.* 2019; Hrnjić *et al.* 2020; Orfanou *et al.* 2020; Orfanou *et al.* 2021; Barfod *et al.* 2024). The samples were mounted on thin glass plates using Blu Tack to make the measurement surfaces as even as possible. The samples remained unpolished during the analysis. The instrument used was the M4 Tornado from Bruker located at the Department of Geoscience, Aarhus University. The X-ray source consists of a rhodium X-ray tube. For the scans, an energy of 50 kV and a current of 600 μA were used. The spot size was set to 20 μm with a measurement time of 25 ms/pixel. The lightest element that can be detected by the instrument is natrium (Na).

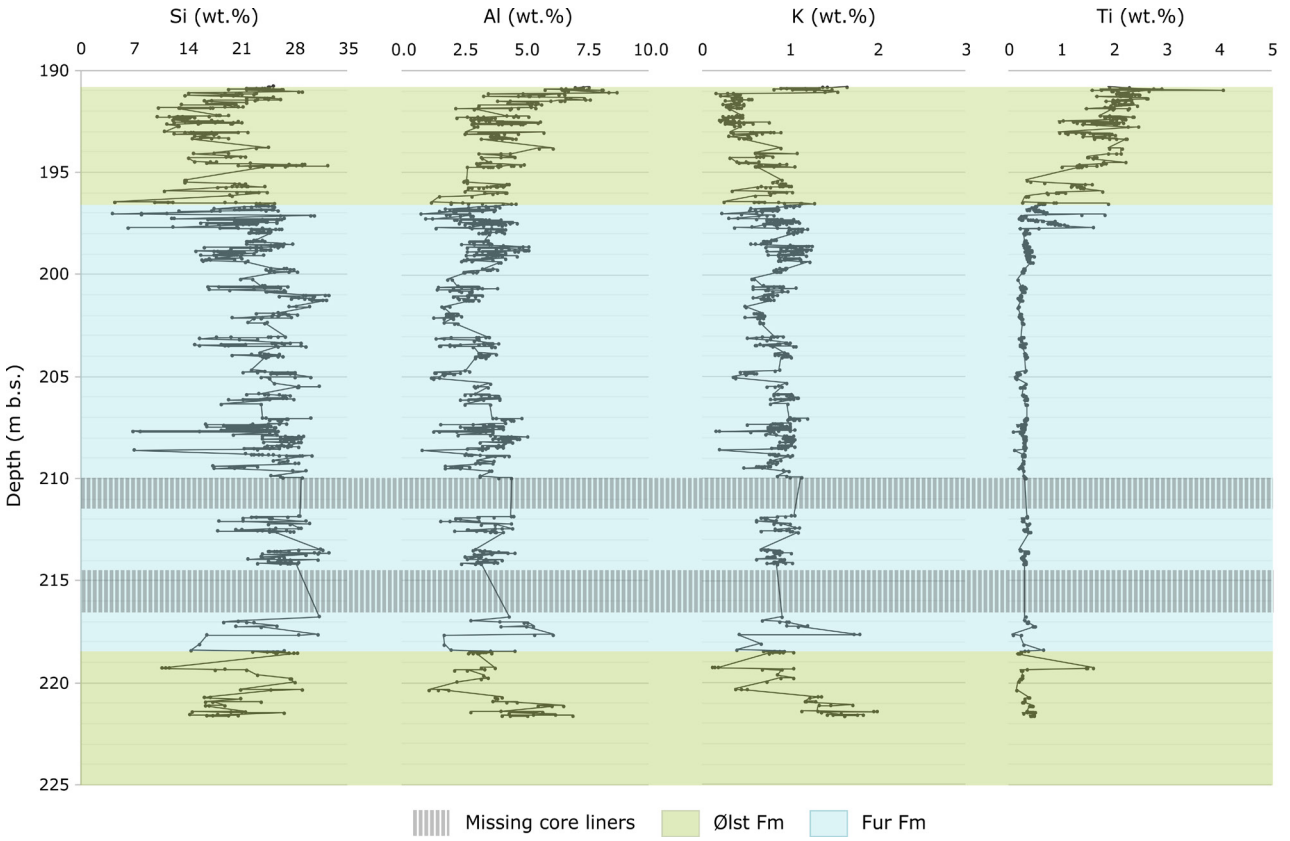

Fig. 3. Depth profiles of the measured concentrations of Si, Al, K, and Ti in wt.%. Missing core liners are marked with grey striped bars. The blue and green intervals indicate the Fur and Ølst Formations defined by Nielsen *et al.* (1994). The depths are uncorrected. The error bars are smaller than the symbols. Precisions remain under 10% for all the elements.

Results

Stratigraphic variations of element concentrations

After processing the HH-XRF data, selected elements were plotted against depth (Figs 3, 4). The concentrations of Si, Al and K oscillate without any major depth trend. However, in the uppermost 5 m within the upper part of the Ølst Formation, an increasing and decreasing trend towards the top can be seen for Al and K, respectively. Conversely, Si exhibits a decreasing trend followed by an increasing trend towards the top. No distinguishable trends are evident in the Fur Formation. In the bottom 3 m in the lower part of the Ølst Formation, despite the relatively few data points, Al and K appear to decrease from bottom to top.

Out of all the elements, Ti shows the most distinct pattern when plotted against depth. The Ti concentrations are near constant from the bottom of the core section at 222 until 198 m b.s. except one outlier between 219 and 220 m b.s., where there is a small peak in concentration. The most notable pattern is the significant variability in Ti concentrations in the upper part of the Ølst Formation with an overall increase in concentration towards the top of the analysed interval. Here, the Ti concentrations are more than 4 folds higher than seen in the base of the section (Fig. 3). A drop in concentration is seen around 195.5 m b.s.

The S, Ca, Fe and Mn content fluctuate significantly (Fig. 4). The S concentrations are highest within the Fur Formation and decrease significantly in the upper part of the Ølst Formation. Between 196 and 198 m b.s. three distinct peaks are visible in the S and Ca profiles. Further down between 207 and 210 m b.s. a pair of peaks can be seen again in both profiles. Distinctive peaks in Mn content are present in this depth interval as well. Between the two missing core liners, the Mn profile exhibits an increase in concentration, which is not as visible in the S and Ca profiles. The Fe depth profile shows fluctuating concentrations overall. However, it can be argued that there is a general increase in Fe from around 200 m b.s. towards the uppermost part of the section. Ca generally seems to increase gradually in the upper part of the Ølst Formation in a similar manner as Ti, Fe and Al.

Geochemical screening and data normalisation

The element depth profiles are highly fluctuating due to the influence of different secondary phases present

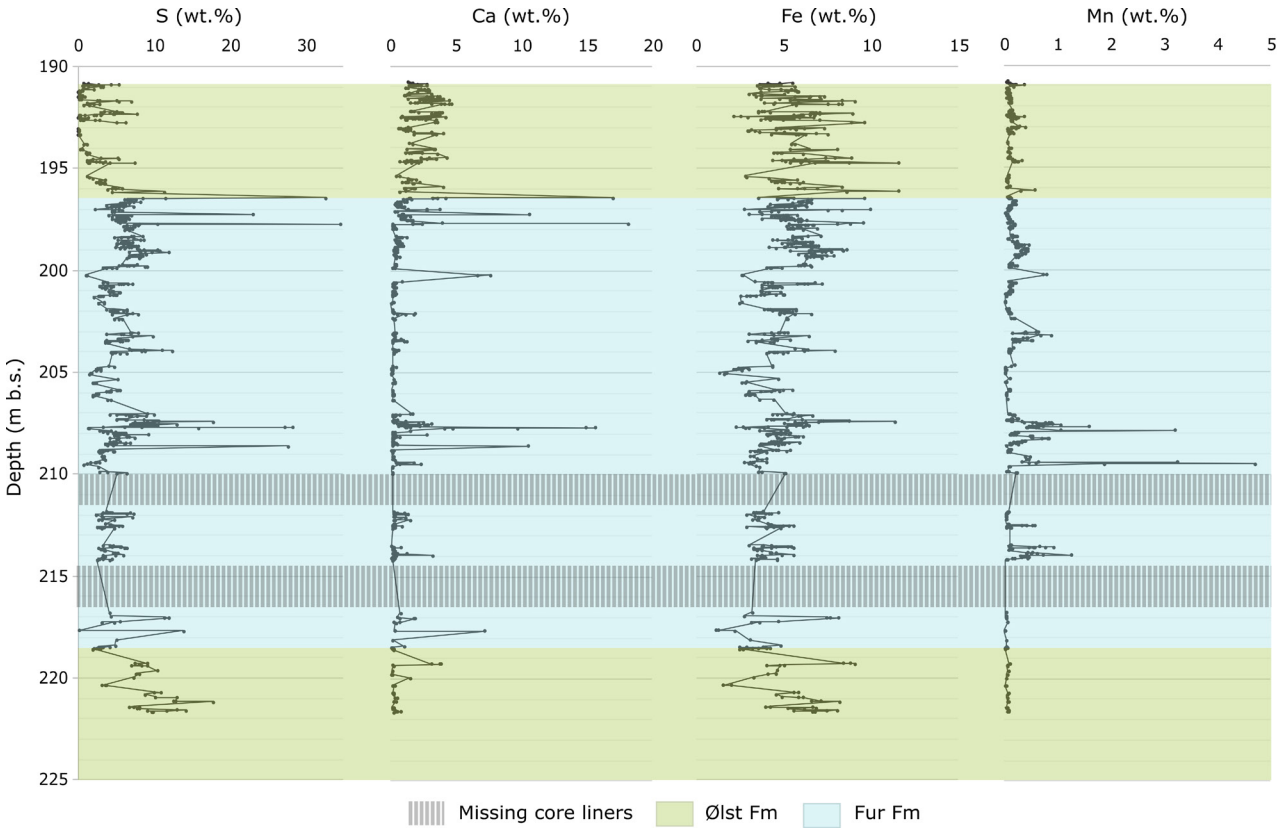

Fig. 4. Depth profiles of the measured concentrations of S, Ca, Fe, and Mn in wt.%. Missing core liners are marked with grey striped bars. The blue and green intervals indicate the Fur and Ølst Formations defined by Nielsen *et al.* (1994). The depths are uncorrected. The error bars are smaller than the symbols. Precisions remain under 10% for all the elements except for S (32.5%).

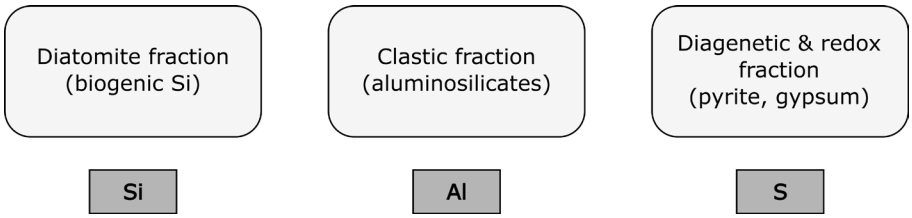

Fig. 5. Schematic diagram of the three normalisations used for the geochemical screening method inspired by Sanei *et al*. (2001). Normalisation to Si is chosen to eliminate the biogenic Si fraction from the bulk data. Normalisation to Al is used to eliminate the clastic fraction (clay). Normalisation to S is used to eliminate the diagenetic and redox fraction caused by the presence of secondary deposits.

in the sediment, which impact the ratios between the elements (Sanei *et al.* 2001). To account for the matrix effect, a geochemical screening method inspired by Sanei *et al.* (2001) was used (Fig. 5), where different normalisations representing their respective fraction are used to eliminate that specific fraction from the data profile, leaving behind the ash signal. In this study, three normalisations are considered to extract hidden patterns as well as the volcanic ash signal in the profiles. Since most of the selected core sections are influenced by the presence of diatomite, a dilution effect caused by biogenic silica needs to be considered, which is accounted for by normalising the XRF data to Si (Fig. 6; Pedersen & Surlyk 1983). The presence of clastic material is also an important fraction to consider, as two clay intervals as well as clay interbedded in the diatomite constitute major parts of the stratigraphy. To eliminate the influence of clastic material from the bulk data, a normalisation to Al is chosen, as Al is a main constituent of aluminosilicates (Fig. 7; Roulet *et al.* 2000; Rimmer 2004). The S depth profile reveals relatively high concentrations of S throughout most of the stratigraphy, except the upper clay interval in the Ølst Formation (Fig. 4). It has long been known that pyrite (FeS_2) and gypsum ($CaSO_4 \cdot 2H_2O$) are frequent in the Fur and Ølst formations (Pedersen *et al.* 1975; Pedersen 2008). Therefore, normalisations of Fe and Ca to S are used to account for diagenetic and redox deposits (Fig. 8). The resulting patterns of the normalisations will be described further below.

Normalisation to Si

For Al/Si and K/Si the normalisations revealed similar patterns within the Fur Formation, where the clastic content fluctuates towards the beginning of

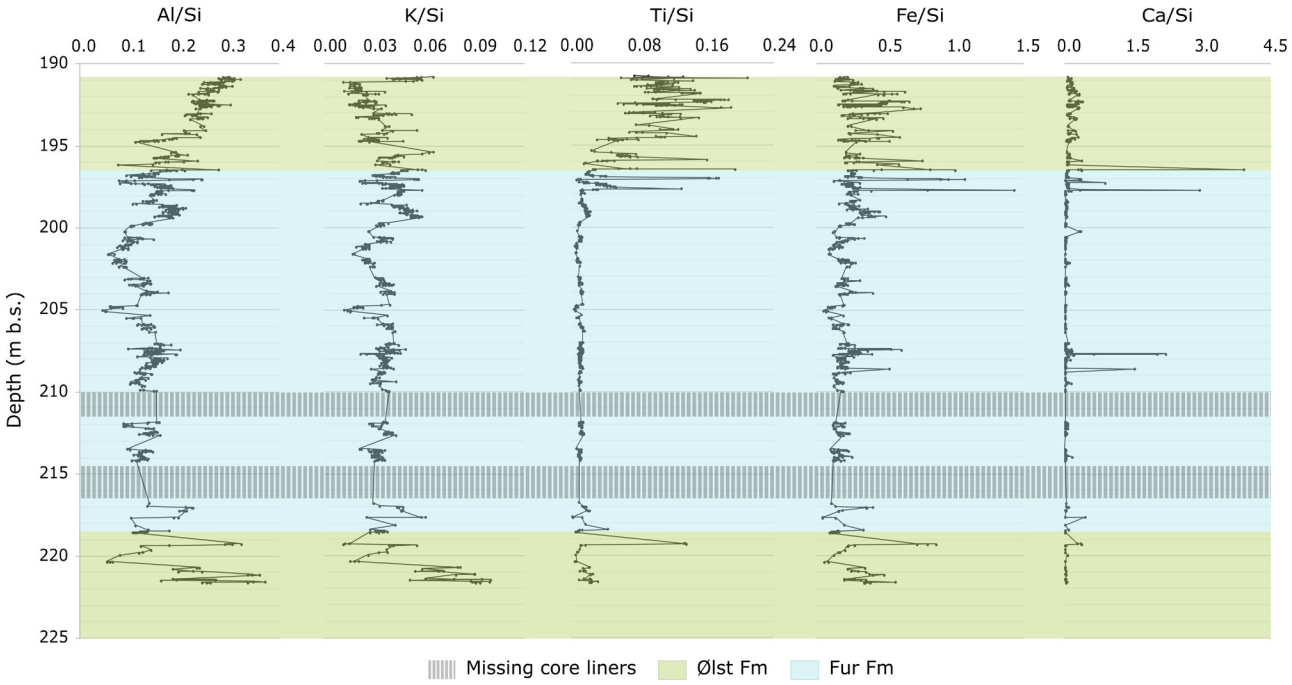

Fig. 6. Normalisation to Si. By normalising to Si, the biogenic silica signals are eliminated from the bulk data. Missing core liners are marked with grey striped bars. The blue and green intervals indicate the Fur and Ølst Formations defined by Nielsen *et al*. (1994). The depths are uncorrected.

the upper part of the Ølst Formation. In the base of the upper part of the Ølst Formation around 196.5 m b.s., the two normalisations show opposite trends, where an increase in the Al/Si ratio and a decrease in K/Si can be seen towards the top of the formation. In the lower part of the Ølst Formation, the compounds show a similar pattern with a decrease in concentration just beneath 220 m b.s., which is instantly replaced by a large increase in both ratios.

The Ti/Si normalisation shows more clearly the increase in Ti concentrations in the upper part of the Ølst Formation where the volcanic ash beds dominate. Four peaks between 195 and 198 m b.s. are even more distinguishable after the normalisation, showing ratios higher than most in the depth profile.

The Fe/Si and Ca/Si normalisations exhibit similar patterns to the Ti/Si profile in the upper part of the Ølst Formation, where they show increasing trends from around 195.5 m b.s. until 193 m b.s., followed by decreasing trends towards the top of the interval. Both Fe/Si and Ca/Si show three-four peaks similar to those seen in Ti and Ti/Si between 195 and 198 m.b.s (Figs 3 and 6). The peaks are absent in the Al/Si and K/Si ratios (Fig. 6). Between 207 and 209 m b.s., two correlating peaks are present in the Fe/Si and Ca/Si ratios, though more prominent in the Ca/Si depth profile. Those peaks are absent in the depth profiles of Al/Si, K/Si, and Ti/Si. In the lower part of the Ølst Formation, a peak is present in the Fe/Si and Ca/Si ratios equal to the one seen in the Ti/Si plot.

Normalisation to Al

The Si/Al depth profile exhibits more clearly the variations in the diatom/clay ratio within the Fur Formation (Fig. 7). This profile particularly illustrates a higher diatom/clay ratio in the 200–203 m b.s. depth interval, as well as at 205 m b.s. Si/Al appears to be constant from approximately 194 m b.s. to the top of the section. Additionally, a significant increase in the ratio is observed at 220 m b.s.

The Ti/Al ratio shows the same increasing trend in the uppermost part of the Ølst Formation. The peaks with relatively high ratios between 195 and 198 m b.s. as well as between 207 and 209 m b.s. reappear in the Fe/Al and Ca/Al depth profiles. The Fe/Al depth profile is otherwise more erratic compared to the Fe/Si ratio and shows no distinct patterns besides a general increase upwards in the depth profile before decreasing again from 195 m b.s. and to the top. The Ca/Al ratio remains close to constant throughout the depth

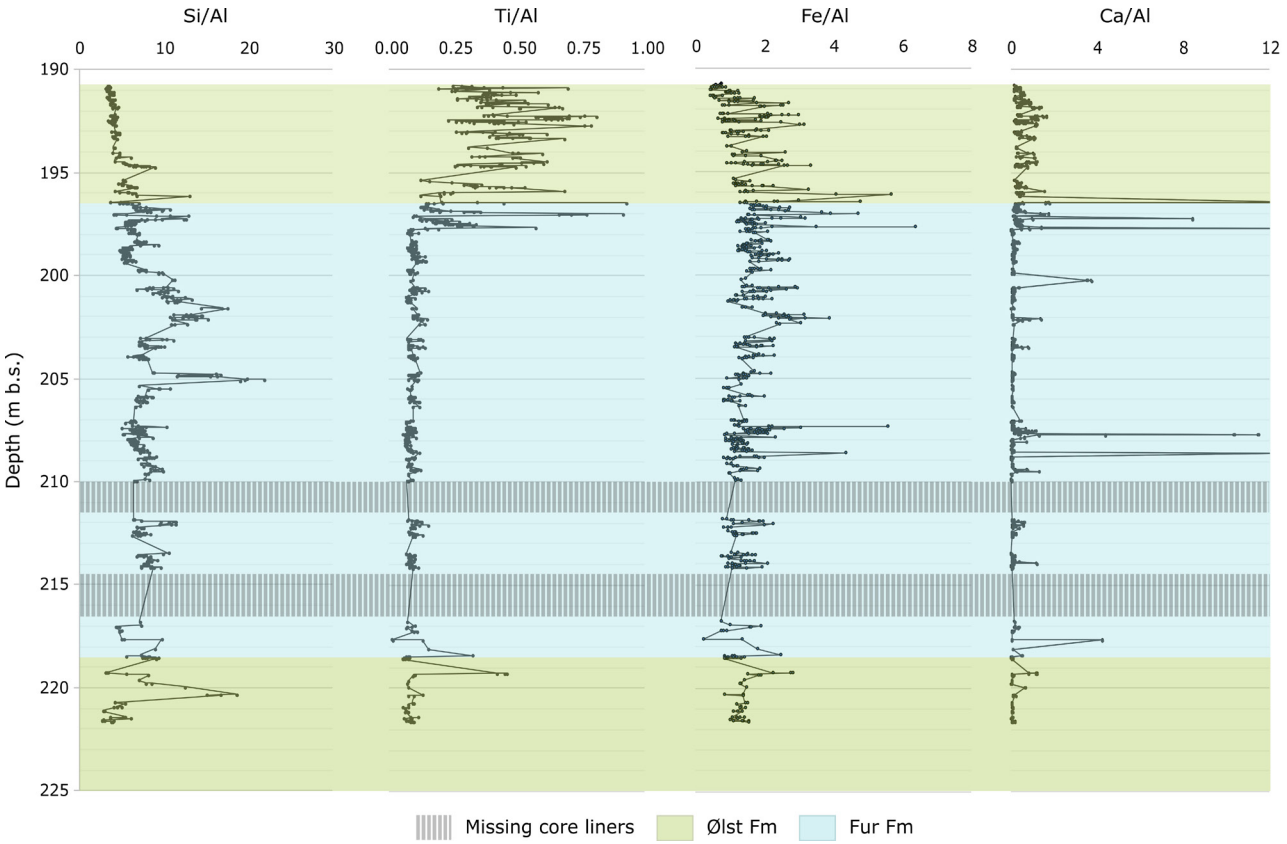

Fig. 7. Normalisation to Al. By normalising to Al, signals caused by the clastic (clay) fraction such as aluminosilicates are eliminated from the bulk data. Missing core liners are marked with grey striped bars. The blue and green intervals indicate the Fur and Ølst Formations defined by Nielsen *et al.* (1994). The depths are uncorrected.

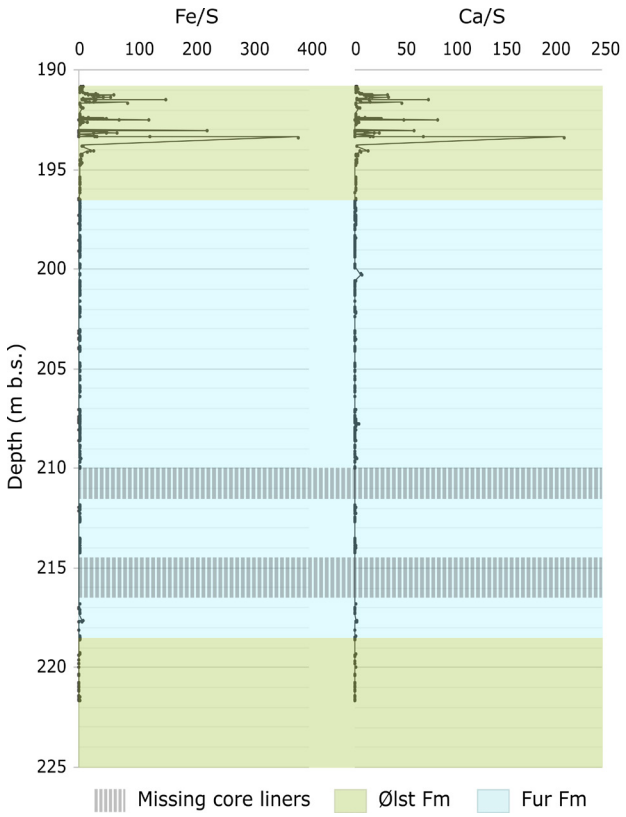

Fig. 8. Normalisation to S. By normalising to S, signals caused by the diagenetic or redox fraction (pyrite and gypsum) are eliminated from the bulk data. Missing core liners are marked with grey striped bars. The blue and green intervals indicate the Fur and Ølst Formations defined by Nielsen *et al*. (1994). The depths are uncorrected..

profile except for the peaks with high increases. In the upper part of Ølst Formation, the Ca/Al ratio displays a similar increase as the Ca/Si ratio.

Normalisation to S

The Fe/S and Ca/S normalisations show similar patterns. Most of the distinct peaks in concentration seen in the Fe/Si, Ca/Si, Fe/Al and Ca/Al normalisations are now eliminated, confirming the presence of diagenetic deposits related to S. From 194 m b.s. and to the top of the section both ratios increase significantly, confirming that most of the Fe and Ca related to other phases such as the volcanic ash are situated in the top of the core section. No such increase is seen in the lower part of the Ølst Formation, suggesting that the increasing content at the uppermost part of the Ølst Formation can be explained by the abundance of volcanic ash beds present here.

Carbon fractionation

The results of the carbon analysis indicate that the total carbon content (TC) in the uppermost part of the Ølst Formation with closely spaced ash intervals ranges between 0.6 and 0.8 wt.%. In contrast, the highest TC content is measured in the lowermost part of the Ølst Formation at 220.24 m b.s., where it reaches a maximum of 3.6 wt.% (Fig. 9A). This depth interval also contains the highest fraction of reactive organic carbon (Fig. 9B).

At 208.98 m b.s., within the Fur Formation, there is a significant decline in both TC and its reactive fraction due to the dilution effect caused by the diatomite. The two intervals above 207.82 m b.s. and 196.79 m b.s. exhibit a progressive increase in TC, particularly in organic and reactive carbon fractions. The highest organic carbon content in the diatomite interval is observed at 196.79 m b.s. at the transition to the upper clay interval with closely packed ash layers. The three uppermost samples in the upper part of the Ølst Formation are characterised by a sharp decline in the TC content and the reactive carbon fraction. In this interval, organic carbon is almost entirely refractory and is likely dominated by detrital organic material.

To further investigate the distribution of different carbon fractions, pie charts are used to represent the respective fraction of the different carbon phases, i.e., reactive organic carbon, refractory organic carbon, and mineral carbon (Fig. 9B). The results show that the samples from the upper part of the Ølst Formation exhibit the highest proportions of mineral carbon relative to the rest of the section, which comprises more than 35% of the TC in the samples taken from 191.12 and 191.27 m b.s. and 57% from the sample at 192.90 m b.s.

Mode of occurrence of elements (elemental affinities)

The PCA of the clr normalised XRF data show that the first three principal components (PCs) model 58.42% of the data variance (PC1: 36.60%, PC2: 13.38%, PC3: 8.44%). The score plots of PC1 vs. PC2

Fig. 9. Sedimentary log and carbon analysis results. **A**. The carbon budgets are given in wt.% of the seven samples at the assigned depths in the stratigraphy (see scale in the legend). The budget is divided into reactive OC, refractory OC, and mineral C. **B**. Pie charts of the carbon fractionation of the seven samples. The samples are shown in order of depth from top to bottom. Depths are uncorrected according to Nielsen *et al*. (1994). The top three samples from the ash-containing interval show the highest fractions of mineral C, while the samples belonging to the Fur Formation and the lower part of the Ølst Formation show higher fractions of reactive and refractory carbon.

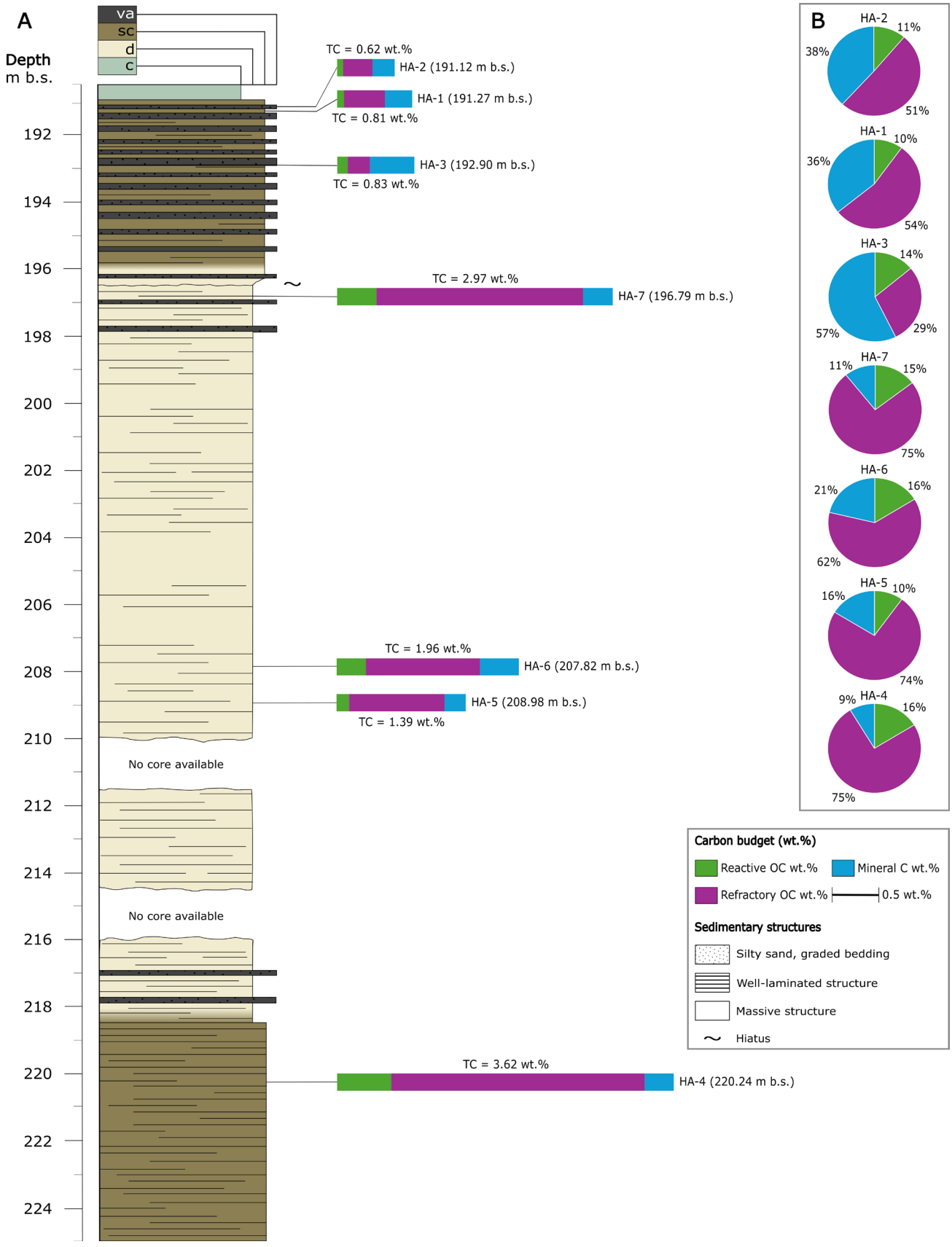
A
Depth
m b.s.
va
sc
d
c
192
194
196
198
200
202
204
206
208
210
212
214
216
218
220
222
224
TC = 0.62 wt.%
HA-2 (191.12 m b.s.)
HA-1 (191.27 m b.s.)
TC = 0.81 wt.%
HA-3 (192.90 m b.s.)
TC = 0.83 wt.%
TC = 2.97 wt.%
HA-7 (196.79 m b.s.)
TC = 1.96 wt.%
HA-6 (207.82 m b.s.)
HA-5 (208.98 m b.s.)
TC = 1.39 wt.%
No core available
No core available
TC = 3.62 wt.%
HA-4 (220.24 m b.s.)
B
HA-2
11%
38%
51%
HA-1
10%
36%
54%
HA-3
14%
57%
29%
HA-7
11%
15%
75%
HA-6
21%
16%
62%
HA-5
16%
10%
74%
HA-4
9%
16%
75%
Carbon budget (wt.%)
Reactive OC wt.%
Mineral C wt.%
Refractory OC wt.%
0.5 wt.%
Sedimentary structures
Silty sand, graded bedding
Well-laminated structure
Massive structure
Hiatus

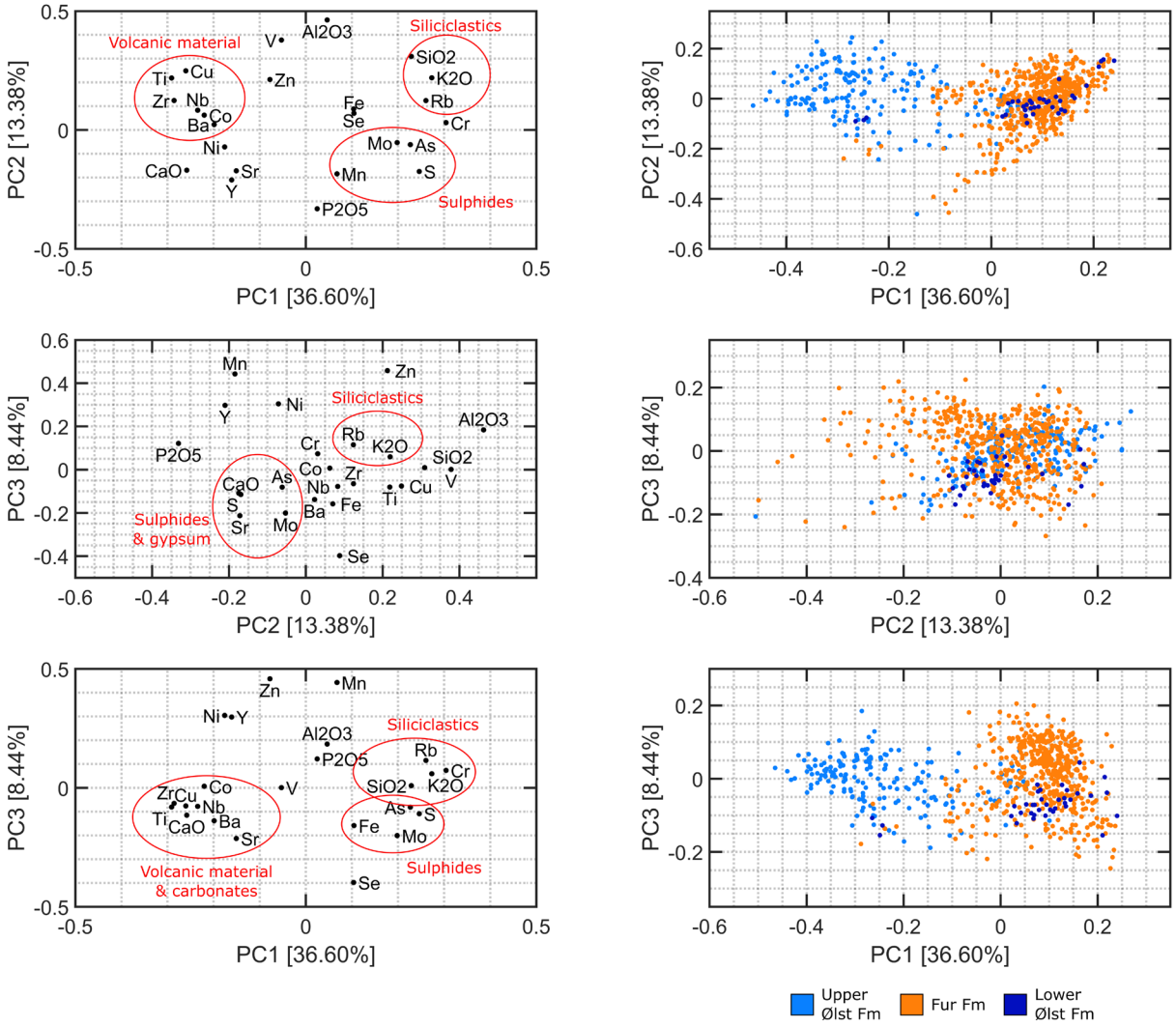

Fig. 10. Principal component analysis (PCA) of the clr normalised, scaled and centred XRF data. The top three principal components of the PCA are plotted against each other in the following order: PC1 vs. PC2, PC2 vs. PC3, and PC1 vs. PC3. The variables and their contributions to the principal components are represented in the left side, while the scores are represented in the right side of the figure. The scores are coloured according to their respective lithological interval as defined by Nielsen *et al*. (1994) (see legend).

and PC1 vs. PC3 show a distinction between samples from the upper part of the Ølst Formation with clay and volcanic ash and the samples of diatomite from the Fur Formation, while the scores belonging to the samples of clay from the lower part of the Ølst Formation plot together with the diatomite from the Fur Formation (Fig. 10). The samples containing clay and volcanic ash within the upper part of the Ølst Formation are characterised by a generally negative PC1, while the diatomite interval from the Fur Formation is distinguished by a positive PC1. In all score plots, a few scores from the Fur Formation plot further away from the general grouping and closer to the scores belonging to the upper part of the Ølst Formation with clay and ash. This is also the case for a few scores belonging to the lower part of the Ølst Formation.

The variables show a clear grouping of Mo, As, and S characterised by a positive PC1, indicating the presence of sulphides. In the PC1-PC3 plot, Fe is also associated with the elements, supporting the occurrence of pyrite. In the PC2-PC3 plot, where the dominating factor is removed, CaO plots together with this grouping, suggesting the presence of gypsum associated with the sulphides. Sr plots close to CaO in all plots characterised by the same negative PC1, suggesting the presence of carbonate minerals as well (Brand *et al.* 1998). Ti, Cu, Zr, Nb, Ba, and Co exhibit another grouping characterised by a negative PC1, which is the same for the scores belonging to the interval rich in volcanic ash. SiO_2 is associated with K_2O, Rb and Cr in all plots defined by a positive PC1 and PC2, indicating mostly siliciclastic or clay-rich material. Compared to the groupings previously

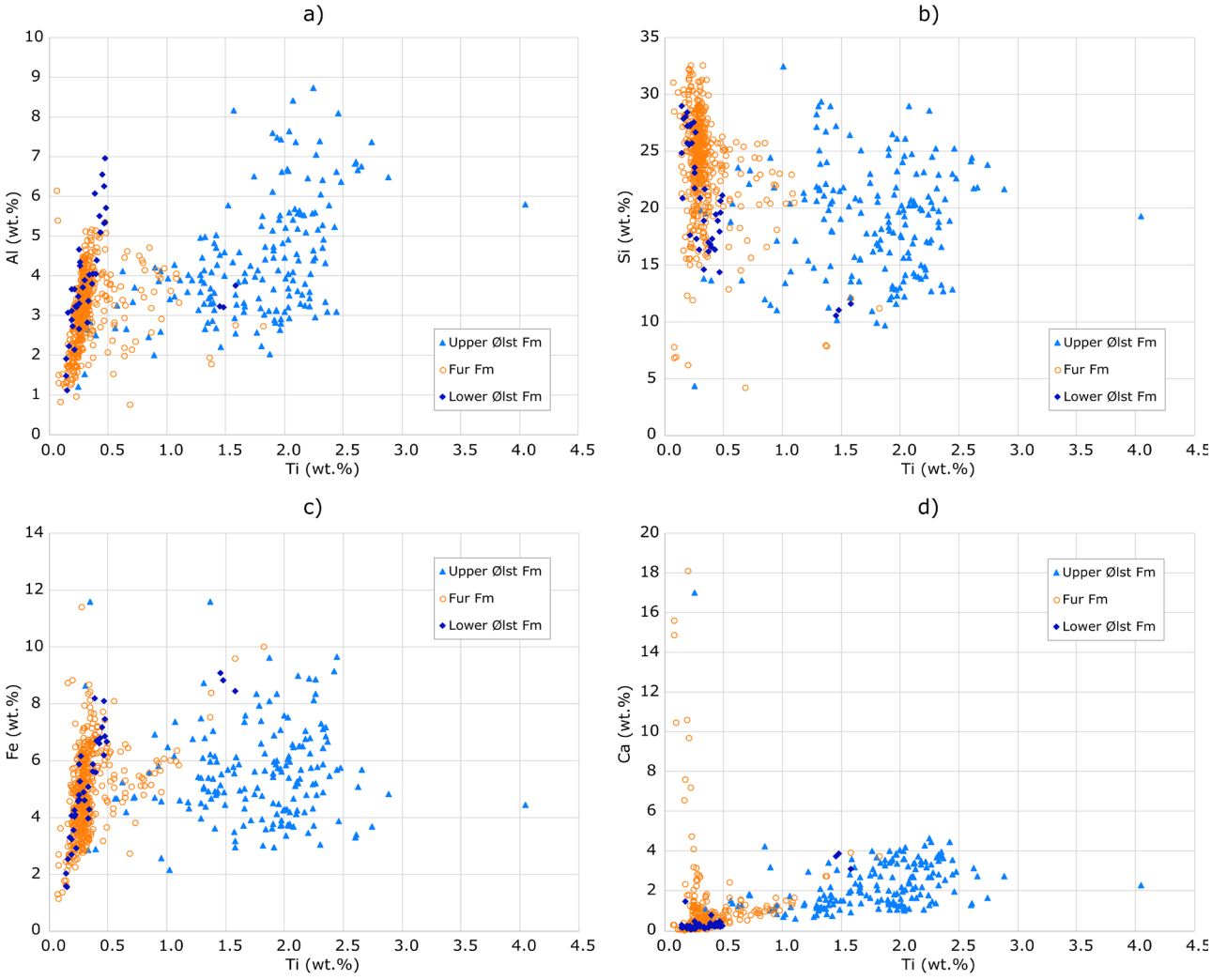

Fig. 11. Cross plots of chosen elements plotted against Ti. a) Al vs. Ti. b) Si vs. Ti. c) Fe vs. Ti. d) Ca vs. Ti. The data have been divided into the intervals of known lithologies, consisting of the upper part of Ølst Formation with volcanic ash beds (light blue triangles), the Fur Formation (orange circles) and the lower part of Ølst Formation (dark blue diamonds). Distinctive trends are most predominant in the Fur Formation and lower part of Ølst Formation with a Ti content below 0.5 wt.%, while the upper part of Ølst Formation shows scattered data points with an elevated Ti content above 0.5 wt.%. The error bars are smaller than the symbols.

mentioned, Al_2O_3 is situated in between and characterised by a positive PC2, showing associations with both the volcanic and siliciclastic materials.

Geochemical facies

For further correlations, selected elements were plotted against Ti, as the results presented above have shown a close relation between Ti and the ash bearing interval. The data have been divided into the same three lithology classes as described earlier in the text (Fig. 11). Ti is a conservative, lithophilic element, while the selected elements can participate in various geochemical reactions (Goldschmidt 1937). Therefore, the cross plots can be used to reveal additional patterns within the dataset, most importantly regarding the volcanic ash.

Common to all four cross plots in Fig. 11 is a clustering of most of the data points situated in the Fur Formation with a Ti content below 0.5 wt.%. For Al and Fe there are positive linear correlations with Ti (Figs 11a and 11c). A positive linear trend between Ca and Ti is also present, though an inverse relationship applies for the data points with a Ca content over 5 wt.% and a Ti content below 0.5 wt.% (Fig. 11d). For Si a negative linear correlation can be seen within the Fur Formation (Fig. 11b). The present data points from the lower part of the Ølst Formation appear to follow the same trends as those within the Fur Formation in all cross plots. A smaller but distinct group of data points within the Fur Formation

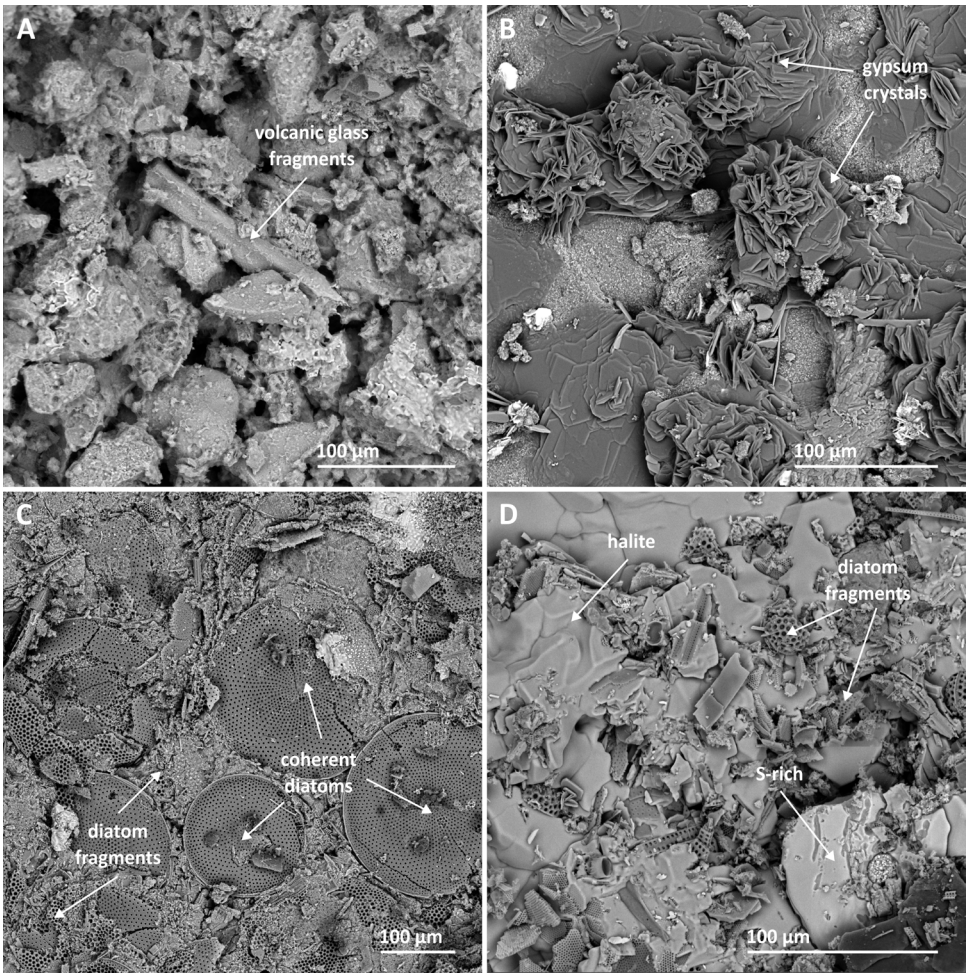

Fig. 12. Backscattered electron images of four of the seven samples taken. **A**. Sample HA-3 from volcanic ash layer +90D showing volcanic glass fragments. **B**. Sample HA-4 from the lower part of the Ølst Formation showing well-developed gypsum crystals. **C**. Sample HA-5 from the Fur Formation showing coherent diatoms and diatom fragments. **D**. Sample HA-7 close to the boundary between the upper part of the Ølst Formation with ash beds and the Fur Formation. The sample shows fragments of diatoms as well as S-rich secondary deposits.

interval appears in the cross plots characterised by elevated Ti varying between 0.5 and 2 wt.%. These outlying data points correspond to a transition into the group of data points belonging to the upper part of the Ølst Formation.

The data points positioned in the upper part of the Ølst Formation appear more scattered and follow no certain type of correlation expect in the Ca-Ti cross plot, where most of the data points arguably follow a positive linear trend (Fig. 11d). The most important characteristic is the enrichment in the Ti content; however, the responding contents of the elements vary. The upper part of the Ølst Formation is enriched in Al as well as Fe and Ca (Fig. 11a and Fig. 11c, d). Si decreases in concentration, as the Ti content increases (Fig. 11b). A few data points belonging to the lower part of the Ølst Formation display Ti contents around 1.5 wt.%.

SEM-EDS and µ-XRF results

Common for nearly all samples is the presence of halite (NaCl), which is evident on both the electron images and µ-XRF area scans. However, sample HA-4 appears not to be influenced by the salt. The halite is believed to be a result of the pore water evaporating from the core during storage. Supplementary descriptions and pictures of the SEM-EDS and µ-XRF results can be found in supplementary file B.

Upper part of the Ølst Formation

Under the SEM, the volcanic ash beds +118 (191.12 m b.s.) and +90D (192.90 m b.s.) (samples HA-2 and HA-3, respectively) show chaotic distributions of volcanic glass fragments characterised by conchoidal fracture planes. The fragments vary in grain size between very fine- and fine-grained sand, and the samples show an overall porous texture (Fig. 12A). Based on the µ-XRF area scans, the volcanic ash shows elevated contents of SiO_2, Al_2O_3, Fe_2O_3, and TiO_2. In layer +118 (HA-2), both CaO and MgO are relatively low compared to layer +90D (HA-3). Besides halite, both ash beds also exhibit phases elevated in S indicating the presence of secondary phases (Fig. 13B).

Sample HA-1, which is taken from a clay layer next

to +118 (191.27 m b.s.), exhibits a lighter and darker phase of which the latter is adjacent to the ash layer. Under the SEM, the sample surface is clearly dominated by halite, however, in the gaps the material consists of unorganized fragments with a plated texture. While the lighter phase of the sample is dominated by halite, the µ-XRF area scan reveals elevated contents of SiO_2, Al_2O_3, Fe_2O_3, and TiO_2 in the darker phase. However, it also exhibits individual phases consisting almost entirely of SO_3 and CaO, suggesting the occurrence of gypsum (Fig. 13A).

Fur Formation

Three samples (HA-5-7) were taken from the Fur Formation at different depths. HA-7, which is taken close to the boundary between the Fur Formation and the upper part of the Ølst Formation (196.79 m b.s.), is chosen based on the peaks seen in the Ca/Si and S/Si depth profiles, which could indicate secondary deposits. The SEM reveals a fragmented matrix consisting of diatoms. In between the diatom fragments, secondary occurrences are present rich in S (Fig. 12D). Samples HA-5 and HA-6 are taken to represent 'clean' diatomite (207.82 and 208.98 m b.s., respectively). Under the SEM, circular coherent diatoms are more frequent (Fig. 12C). The diatomite matrix for all three samples is well defined by the µ-XRF area scans by a high SiO_2 content (Fig. 13D). The secondary phases consist mostly of equal amounts of CaO and SO_3 indicating gypsum, while others are dominated by either Ca or S (Figs 13D-E). HA-7 is more elevated in Fe compared to HA-5 and HA-6.

Lower part of the Ølst Formation

Sample HA-4 origins from the lower part of the Ølst Formation, where volcanic ash beds are very limited (220.24 m b.s.). The SEM has revealed distinct rose-shaped crystals throughout the sample surface, a well-known characteristic for gypsum crystals (Fig. 12B; Ralph *et al.* 2025). The matrix of the sample is more compact compared to the clay layer in sample HA-1

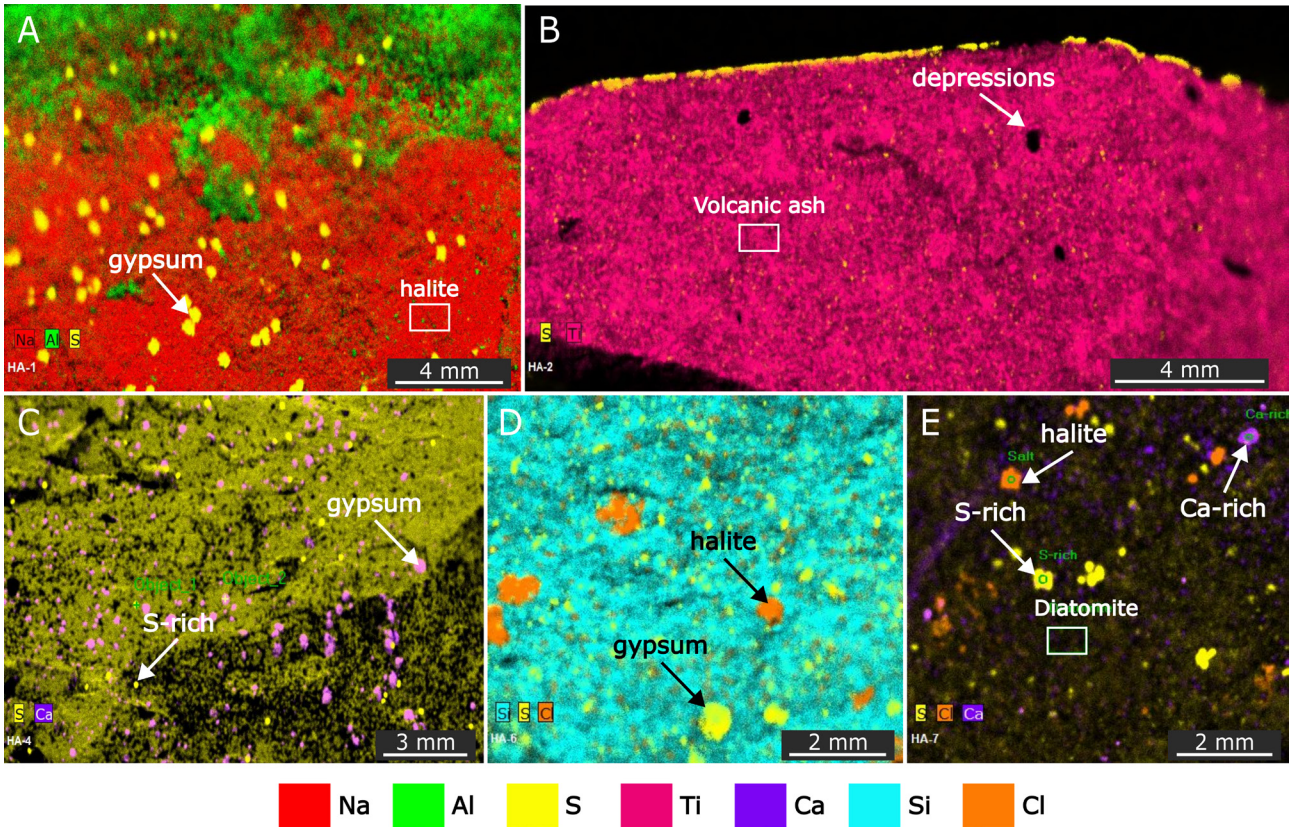

Fig. 13. µ-XRF area scans of five of the seven samples taken. **A**. Sample HA-1 from a clay layer in between ash beds in the upper part of the Ølst Formation. The area scan reveals gypsum occurrences in the pore spaces of the sample. **B**. Sample HA-2 from volcanic ash layer +118. While the area scan shows elevated concentrations of Ti, it also reveals secondary deposits rich in S. **C**. Sample HA-4 from the lower part of the Ølst formation. S dominates the sample, confirming the occurrences of pyrite and gypsum. **D, E**. Samples HA-6 and HA-7 from the Fur Formation. Among the diatom matrix secondary deposits like gypsum and halite are present.

and show very low porosity. The μ-XRF area scan reveals that the sample contains little SiO_2 and is dominated by S, Fe_2O_3, Al_2O_3 and Na_2O (Fig. 13C). Smaller phases equally rich in CaO and SO_3 confirm the presence of the gypsum crystals, while other phases contain mostly S. The high contents of S and Fe indicate that the presence of pyrite dominates the sample.

Discussion

Geochemical proxy for volcanic ash

The depth profile of Ti shows the most distinct geochemical trends for the normalised XRF data, separating the upper part of the Ølst Formation with volcanic ash from the rest of the core section. The PCA and cross plots have further supported the distinction of the upper part of the Ølst Formation with volcanic ash from the Fur Formation and lower part of the Ølst Formation. Ti is well known to be incorporated in marine sediments (Calvert & Pedersen 2007), and it is therefore essential to determine whether the elevation in Ti is a consequence of a change in clay mineral assemblage or caused by the volcanic ash beds. This can be accomplished by calculating enrichment factors (EF) of Ti. The enrichment factors will be based on Al ratios of the XRF measurements with reference to the average composition of deep-sea sediment (Eq. 3) (Turekian & Wedepohl 1961; Taylor & McLennan 2003; Calvert & Pedersen 2007).

$$EF\,(Ti) = \frac{\frac{Ti}{Al}}{\frac{Ti_{ref}}{Al_{ref}}} \qquad (3)$$

Depth variations of the estimated EFs of chosen elements have been calculated in this study (Fig. 14). The EF(Ti) profile shows enrichment of greater than seven times relative to the average pelagic sediment. This high enrichment of Ti coincides with the upper part of the Ølst Formation containing volcanic ash beds, which clearly indicates that the enrichment in Ti is due to the presence of volcanic ash rather than normal sedimentary processes. Titanium is known to be a conservative, lithophilic element, which is relatively immobile in surface environments due to the 4+ valence (Winchester & Floyd 1977; MacLean & Barrett 1993).

The geochemical compositions of the volcanic ash beds also need to be considered, as the origins of the individual beds are related to different stages of volcanism (Pedersen *et al.* 1975; Morton & Evans 1988; Morton & Knox 1990; Larsen *et al.* 1999; Larsen *et al.* 2003; Stokke *et al.* 2020; Stokke *et al.* 2021; Jones *et al.* 2023). The ash beds of the positive series are especially known to differ from the older beds of the negative series. Besides a few beds of rhyolitic composition, the positive series mainly consists of ferrobasalts with a Fe-Ti-rich tholeiitic composition (Larsen *et al.* 2003) reflected in our data by the elevated concentrations in Ti in the top of the core section, where the ash beds of the positive series are situated. The ash beds of the negative series have widely different compositions (trachyte, rhyolite and alkaline basalts) and are often heavily altered, based on the amount of volatile contents present (Larsen *et al*. 2003). Since the Ti concentrations in the negative series are generally low compared to the positive series due to Ti fractionation, Ti is not necessarily the best indicator for identifying the older ash beds.

The presence of divalent cations in the Harre borehole

The most important factor for the possibility of carbon mineralisation is the presence of free divalent cations (Ca^{2+}, Mg^{2+}, Fe^{2+}) necessary for reacting with dissolved CO_2 (carbonic acid) and precipitating carbonate minerals (Snæbjörnsdóttir *et al.* 2020). Contrary to Ti, which is a relatively immobile element, divalent cations can be leached out of the ash due to alteration processes (Pedersen & Buchardt 1996; Larsen *et al*. 2003; Longman *et al.* 2021). Compared to the Fur Formation, where the ash beds are known to be well-preserved in diatomite, the same ash beds are recognized as heavily altered in the clay-rich Balder and Sele formations from the North Sea as well as in the onshore Ølst Formation of equal age (Heilmann-Clausen *et al.* 1985; Huggett 1993). Since the volcanic ash beds are mostly situated within a clay interval equal to the Ølst Formation in the Harre borehole, there is a possibility that the beds have undergone alteration in contrast to the well-preserved ash beds imbedded in diatomite farther north (Güven & Grim 1978; Pedersen *et al*. 2011). It is therefore crucial to determine whether the divalent cations are still present or have been leached out of the subsurface volcanic ash beds.

Magnesium measurements have proved unsuitable for evaluating the presence of divalent cations in the Harre drill core, as most of the measured concentrations were below the detection limit (supplementary file A). Calcium is an important cation in terms of carbon mineralisation, and the enrichment of Ca in the upper part of the Ølst Formation is therefore a key piece of information for further development of a potential carbon mineralisation facility in the area. The depth variations of Ca and Fe both show a gradual increase in the upper part of the Ølst Formation similar to Ti normalised to S, which suggests that the increase of Ca and Fe in the uppermost part

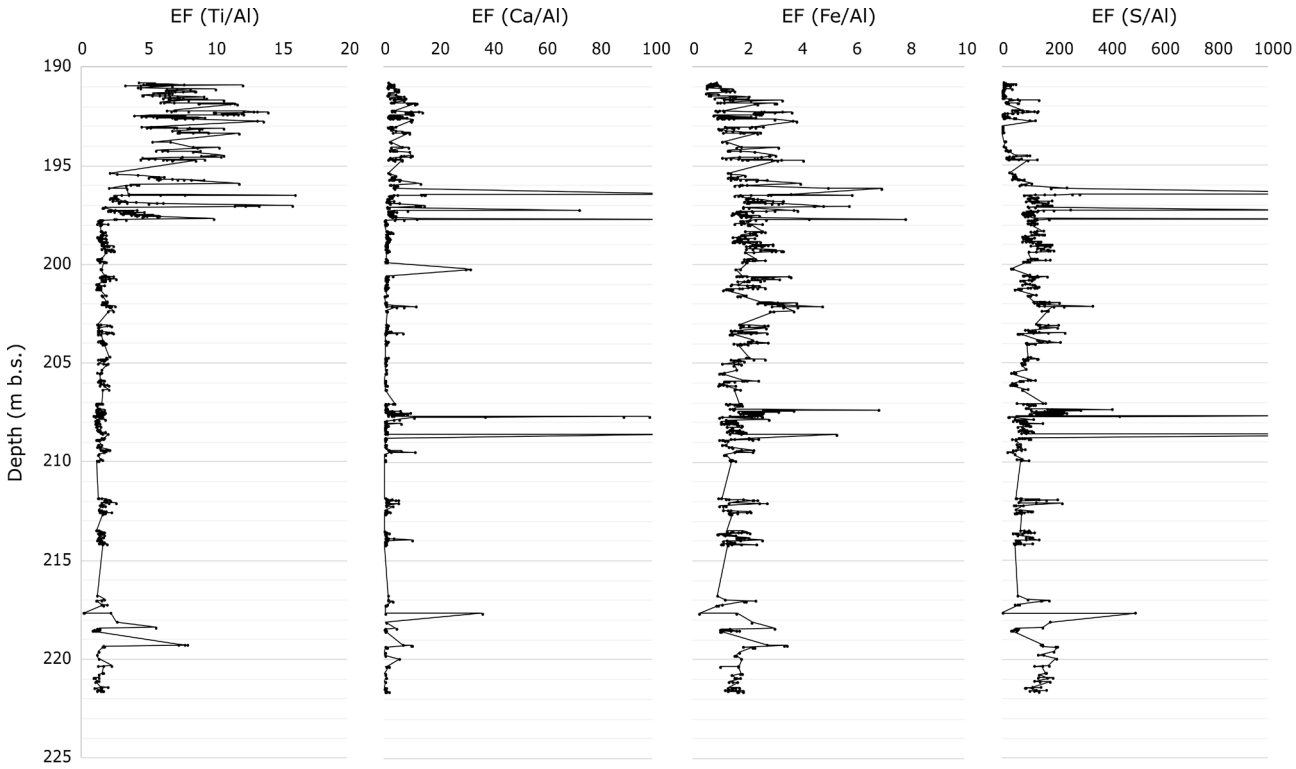

Fig. 14. Chosen Enrichment Factors (EF) based on chosen Al ratios. The reference values used for the EF calculations are based on the elemental concentrations in pelagic sediments from Taylor & McLennan (2003). The most significant enrichments are seen in Ti and Ca, which are mostly limited to the ash-containing interval in the top of the core section.

of the Ølst Formation is related to non-diagenetic deposits, likely associated with volcanic ash. Despite the extreme enrichments of Ca associated with the gypsum horizons within the Fur Formation, the ratio is more uniformly enriched in the upper part of the Ølst Formation with volcanic ash. This is not the case for the lower part of the Ølst Formation, where the enrichment is limited (Fig. 14). The enrichment seen in the upper part of the Ølst Formation therefore indicates the influence of Ca in the volcanic ash. The EF(Fe) shows an overall increasing trend towards the top of the core section; however, it is difficult to assign the enrichment to any specific phases as the pattern fluctuates significantly. Since Fe is a common constituent in clay-rich sediments as well as in diagenetic phases like pyrite, this may influence on the general Fe trends (Stucki 2013). HH-XRF determines total Fe, and therefore it is uncertain which oxidation level defines the present Fe in the core.

Gypsum deposits – potential mapping of Ca mobility

Gypsum and pyrite are commonly found in outcrops of the Fur Formation and the underlying Stolleklint Clay (Pedersen *et al.* 1975; Pedersen 2008; Pedersen *et al.* 2011). In the Harre borehole, this is the case as well. Especially gypsum has been found throughout the analysed core section, which is best demonstrated by the SEM-EDS and μ-XRF data. The gypsum found in most of the samples are visible on the μ-XRF area scans, while sample HA-4 from the lower part of the Ølst Formation clearly illustrates coherent gypsum crystals with SEM-EDS (Fig. 12B). The occurrences of gypsum reflect the mobility of Ca within the present Ash Series and is further discussed in the text below.

Pyrite oxidation

Studies of diatomite outcrops on the island of Fur indicate that gypsum deposits can be explained by the oxidation of pyrite (Pedersen *et al.* 1975; Pedersen 2008). Above the redox level, pyrite is oxidized primarily by O_2, producing sulphate ions (SO_4^{2-}; Eq. 4–6; Moses & Herman 1991; Chandra & Gerson 2010). This leads to the precipitation of minerals such as jarosite ($KFe_3(SO_4)_2(OH)_6$) and gypsum ($CaSO_4{\cdot}2\,H_2O$; Pedersen 2008).

$$FeS_{2(s)} + \frac{7}{2}\,O_{2(aq)} + H_2O_{(l)} \rightarrow Fe^{2+}_{(aq)} + 2\,SO^{2-}_{4\,(aq)} + 2\,H^{+}_{(aq)} \quad (4)$$

$$FeS^{2+}_{(aq)} + \frac{1}{4}\,O_{2(aq)} + H^{+}_{(aq)} \rightarrow Fe^{3+}_{(aq)} + \frac{1}{2}\;H_2O_{(l)} \quad (5)$$

$$FeS_{2(s)} + 14Fe^{3+}_{(aq)} + 8H_2O_{(l)} \rightarrow 15Fe^{2+}_{(aq)} + 2SO^{2-}_{4(aq)} + 16H^{+}_{(aq)} \quad (6)$$

For the sulphate ions to precipitate as gypsum, Ca^{2+} ions need to be available, which is happening naturally by the weathering and alteration of Ca bearing phases (Berner *et al.* 1983; Berner 1999, 2004). A possible source of Ca in the Harre core could be the volcanic ash beds. The altered ash beds found in the clay-rich formations in the North Sea and in the onshore Ølst Formation lead to the suspicion that the volcanic ash in the Harre core might have experienced alteration as well, given that they are mostly situated in clay instead of diatomite. It is, however, evident from earlier studies of the volcanic ash beds within the Harre core that many of them remain unaltered (Hansen 2018). Additionally, the Ca participating in the formation of calcareous concretions in the Fur Formation has partly been attributed to blooms of calcareous plankton, dissolution of skeletal material from fish and invertebrates, and volcanic dust dispersed in the diatomite (Pedersen & Buchardt 1996). The above-mentioned serve as additional possible sources of Ca for the precipitation of gypsum and more likely, as they are more abundant than the ash.

Sample HA-4 comes from the lower part of the Ølst Formation. This interval shows high content of pyrite and organic matter, resulting in a relatively high gamma ray signal, and can be attributed to the Stolleklint Clay (Nielsen *et al*. 1994; Heilmann-Clausen 1995; Schiøler *et al*. 2007). The results of the SEM-EDS and μ-XRF analyses of sample HA-4 reveal high contents of both pyrite and gypsum. We suggest that the gypsum occurrences seen throughout the Harre core, and particularly in sample HA-4, are a result of pyrite oxidation occurring in the lower part of the Ølst Formation. From there, it is possible that the released sulphate ions have been transported by the formation fluid farther up in the stratigraphy due to the high porosity of the diatomite (~70%; Pedersen *et al*. 2011).

The older volcanic ash beds (–28 to –34) present at the bottom of the Fur Formation are also of basaltic origin, however heavily altered and less enriched in TiO_2, K_2O, and P_2O_5 compared to the younger ferro-basaltic beds in the upper part of the Ølst Formation (Larsen *et al.* 2003). It is possible that the Ca has leached out of the older ash beds and thereby contributing to the precipitation of gypsum as well, which will be discussed below.

Potential leaching and mineralisation of Ca

The relatively low S content in the upper part of the Ølst Formation shows a trend of significant meaning. The EF(S) profile indicates depletion in S in this interval compared to the average pelagic sediment (Fig. 14). This could indicate that the precipitation front of gypsum has not yet reached the top interval with the volcanic ash beds. This is further supported by the SEM-EDS and μ-XRF findings, where halite is clearly dominating the pore spaces.

The positioning of positive peaks between 196 and 198 m b.s. in the Ca and S profiles, as well as their respective Si normalisation profiles occur between the peaks seen in the Ti/Si profile (Fig. 15). Some of the volcanic ash beds in this interval (–11 to –13) are known to exhibit similar geochemical trends to the ash beds of the positive series above, however, more enriched in Si and Ti (Larsen *et al.* 2003). This could explain the peaks seen in the Ti normalisations from this interval. The peaks in the S/Si and Ca/Si ratios as well as in the EF(Ca) and EF(S) located in between the Ti peaks could therefore indicate the leaching and reprecipitation of Ca from the surrounding volcanic ash beds.

Pyrolysis analysis has further revealed the presence of mineral-stored carbon, suggesting that carbonates have formed. This is especially the case for the ash bearing interval in the upper part of the Ølst Formation, which exhibits mineral carbon fractions above 35% of the total carbon contents (Fig. 9). These results provide strong evidence for past mineralisation within the volcanic ash. The potential leaching of Ca from the volcanic ash could be of concern for the potential of carbon mineralisation. The Ca^{2+} is considered one of the important cations for the mineralisation of CO_2, and it is therefore crucial that as much Ca as possible remains available. Though the established gypsum occurrences show evidence of leaching of Ca, it is also obvious that the Ca content remains high among the volcanic ash beds in the top relative to the rest of the core section (Fig. 16). It is also important to address that the total carbon content measured throughout the core section is low (Fig. 9). Especially in the ash bearing interval in the upper part of the Ølst Formation, the TOC content is relatively low due to dilution by siliciclastic volcanic materials. These findings suggest that a significant potential for further mineralisation remains, despite the findings of past mineralisation in the ash.

It is equally important to consider the fact that the core sections have been stored for many years and dried out completely. During storage, it is likely that most of the pyrite present in the core has been oxidized and reprecipitated as gypsum over time. Additionally, the previous studies of the Harre drill core by Nielsen *et al.* (1994) report no occurrences of gypsum in the ash-bearing interval from the fresh core samples. It is therefore likely that most of the gypsum precipitated during storage of the core.

Since the HH-XRF measurement error of the S standard is high (33%), there is a risk of over interpreting the elevated peaks in the S depth profile. However, the Ca standard HH-XRF measurements show a relatively low measurement error (precision=7%).

Since the Ca depth profile shows the same trends as in S, it is evident that the peaks are not simply errors in the handling of the HH-XRF instrument. As the average Ca concentration of the used standard was unavailable, it is difficult to estimate the accuracy of the HH-XRF measurements. It is emphasized that the geochemical data presented in this study were created to provide an overview of the distribution of elements and compounds throughout the analysed core sections. They should therefore not be considered presentable of the actual quantities of Ca, especially regarding the volcanic ash beds. In the future, it will be crucial to examine the amount of free divalent cations in the volcanic ash to provide a better estimate of the quantity of CO_2 that can be stored through carbon mineralisation in the region.

Implications – carbon storage potential of the ash beds

Based on the results of this study, the ash beds show a large potential for carbon mineralisation. The ash beds are closely spaced in the top 5 m of the analysed core interval, which therefore defines the main target zone for the process to take place. A reservoir of this thickness with widespread geographical coverage in a large area in Jylland has significant mineralisation potential. The vision of the C·ASH project is to utilise the large geographical coverage of the ash beds to connect distributed local sources of CO_2 from smaller capture facilities like biogas. Thereby a larger number of CO_2 sources may potentially be directly integrated with mineralisation in the future. The fact that

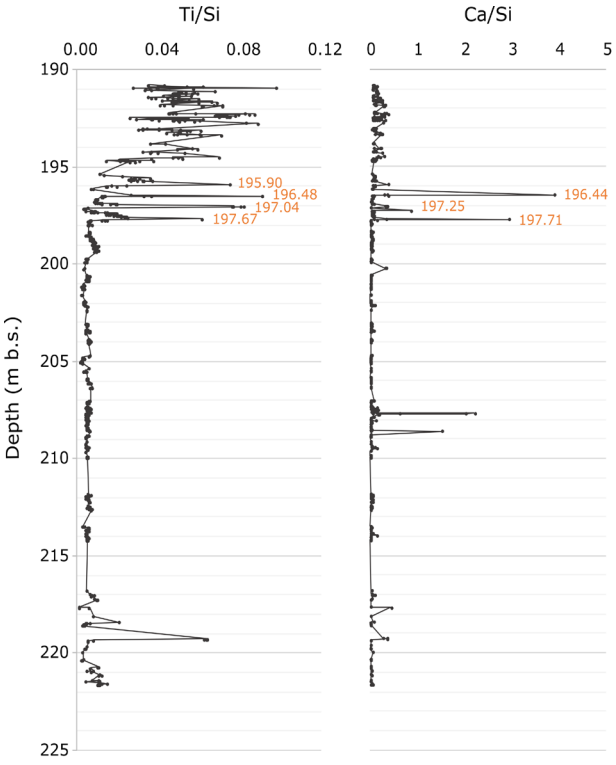

Fig. 15. Ti/Si and Ca/Si depth profiles. The depths of the elevated ratios between 196 and 198 m b.s. in both profiles are provided. It is evident from the depth points that the peaks in Ca/Si are situated in between the peaks in Ti/Si, suggesting leaching and redeposition of Ca as gypsum.

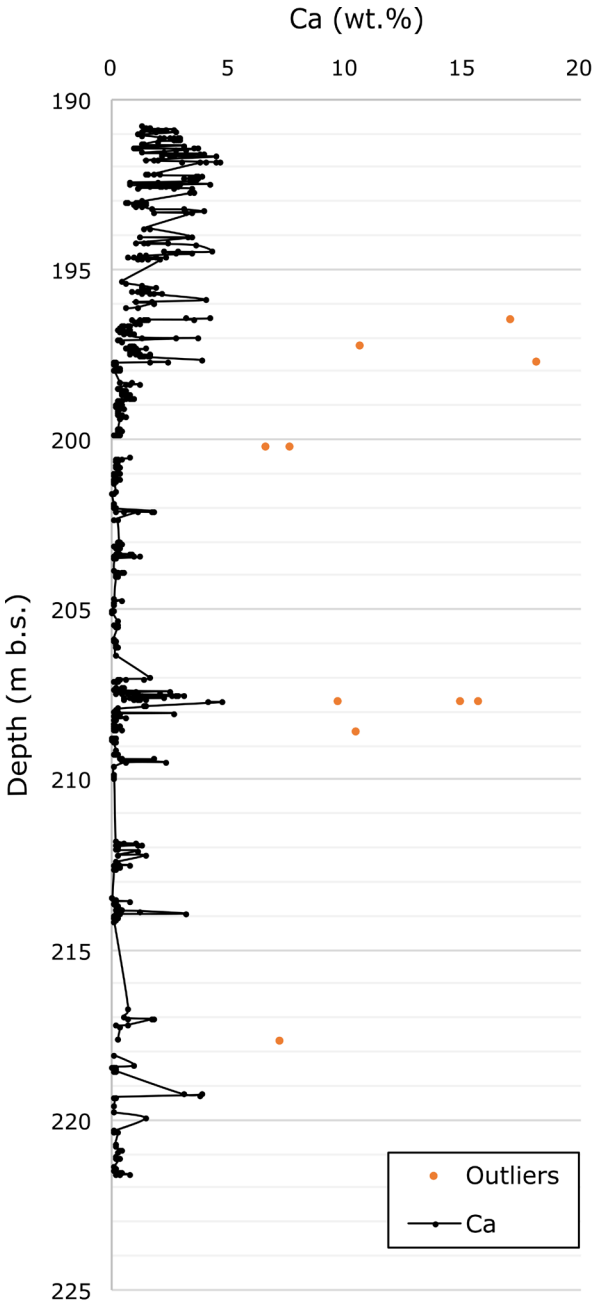

Fig. 16. Profile showing the distribution of Ca throughout the core section. Outliers identified as gypsum are presented with orange dots to better illustrate the increase of Ca associated with volcanic ash in the upper part of the Ølst Formation. The error bars are smaller than the symbols. The precision for Ca is 7%.

the ash beds are more closely packed in the Harre borehole compared to the outcrops on Fur could prove to be advantageous, as a more focused target zone may support more efficient water flow and mineralization. The results of this study show that the Ti-Fe basalts situated in the target zone clearly have a higher content of Ca compared to the rest of the ash beds, making the target zone even more suitable for carbon mineralisation. The analysed ash beds (+90D and +118) furthermore exhibit low degrees of weathering, even though they are situated in clay instead of diatomite. However, important questions related to the hydrological properties of the target zone remain to be answered, which requires further studies regarding the permeability and porosity of the sediments and ash.

Conclusion

Through the selected geochemical analyses of the core section, Ti has proven to be the best elemental proxy for volcanic ash due to a distinct association with the ash beds of the positive series identified in the core. The high content of the highly conservative element Ti is a signature of the positive series. It is therefore considered a stable indicator of the Ti-Fe basaltic ash beds. The results show that the majority of the present ash beds are situated in the top 5 to 6 m of the core section, where they are interbedding with clay from the Ølst Formation instead of diatomite from the Fur Formation, contrasting to the outcrops seen on the island of Fur. Previous studies of the Harre borehole by Nielsen *et al*. (1994) also revealed an interfingering stratigraphy between the Fur and Ølst formations.

The divalent cation of calcium (Ca^{2+}) is an essential driver of the carbon mineralisation reaction, which is evidently enriched in the uppermost part of the Ølst Formation, associated with volcanic ash from the positive series. However, this study also shows that Ca can be incorporated in authigenic minerals such as carbonates and gypsum. We suggest that these secondary minerals reveal the mobility of Ca and possibly some degree of leaching from the volcanic ash. Based on the results of this study and previous studies, the fraction of secondary minerals is believed to be minimal, as the degree of alteration in the ash layers remains low. The ash layers are therefore still considered highly suitable for carbon sequestration, a key asset for the C·ASH project.

Acknowledgements

This study was funded by the Aarhus University Research Foundation. We would like to thank Dr. Rasmus Andreasen (Aarhus University) for help in instructing us in the use of the HH-XRF instrument and μ-XRF. A warm thank you to Astrid Rosenberg Hansen (Copenhagen University) for her immense help with the PCA. We would also like to thank Trine Ravn-Jonsen (Aarhus University) for assisting the sample preparation and execution of SEM-EDS. Constructive and positive comments by journal referees Claus Heilmann-Clausen and Maja Bar Rasmussen helped to improve the manuscript.

References

Aitchison, J. 1984: The statistical analysis of geochemical compositions. Journal of the International Association for Mathematical Geology 16, 531–564. https://doi.org/10.1007/BF01029316.

Andersen, S.A. 1937: De vulkanske Askelag i Vejgennemskæringen ved Ølst og deres Udbredelse i Danmark. Danmarks Geologiske Undersøgelse II. Række 59, 52 pp. https://doi.org/10.34194/raekke2.v59.6847

Aradóttir, E.S.P., Sigurdardóttir, H., Sigfússon, B. & Gunnlaugsson, E. 2011: CarbFix: A CCS pilot project imitating and accelerating natural CO2 sequestration. Greenhouse Gases: Science and Technology 1, 105–118. https://doi.org/10.1002/ghg.18

Baklid, A., Korbol, R. & Owren, G. 1996: Sleipner Vest CO2 disposal, CO2 injection into a shallow underground aquifer. Paper presented at SPE Annual Technical Conference and Exhibition, October 6. https://doi.org/10.2118/36600-MS

Barfod, G.H., Feveile, L.L. & Sindbæk, S.M. 2024: The Emperor's new glass: The introduction of Carolingian wood ash glass in North Sea trade. Archaeometry 66, 534–551. https://doi.org/10.1111/arcm.12968

Berner, R.A. 1999: A new look at the long-term carbon cycle. GSA TODAY - A publication of the Geological Society of America 9, 1–6.

Berner, R.A. 2004: The Phanerozoic carbon cycle: CO2 and O2. Oxford University Press. https://doi.org/10.1093/oso/9780195173338.001.0001

Berner, R.A., Lasaga, A.C. & Garrels, R.M. 1983: The carbonate-silicate geochemical cycle and its effect on atmospheric carbon dioxide over the past 100 million years. American Journal of Science 283, 641–683. https://doi.org/10.2475/ajs.283.7.641

Birch, T., Orfanou, V., Lichtenberger, A., Rubina, R., Barfod, G.H., Lesher, C.E., Schulze, I. & Schulze, W. 2019: From Nummi Minimi to Fulūs—small change and wider issues: Characterising coinage from Gerasa/Jerash (Late Roman to Umayyad periods). Archaeological and Anthropological Sciences 11, 5359–5376. https://doi.org/10.1007/s12520-019-00866-9

Bøggild, O.B. 1918: Den vulkanske Aske i Moleret samt en Oversigt over Danmarks ældre Tertierbjergarter. Danmarks Geologiske Undersøgelse II. Række 33, 159 pp. https://doi.org/10.34194/raekke2.v33.6818

Bonde, N. 1973: Fiskefossiler, diatomiter og vulkanske askelag. Dansk Geologisk Forening Årsskrift for 1972, 136–143.

https://2dgf.dk/xpdf/dgfaars1972-136-143.pdf
Bonde, N. 1974: Palaeoenvironment as indicated by the 'Mo-Clay Formation' (Lowermost Eocene of Denmark). Tertiary Times 2, 29–36.
Bonde, N. 1979: Palaeoenvironment in the 'North Sea' as indicated by the fish bearing Mo-Clay deposit (Paleocene/Eocene), Denmark. Mededelingen van de Werkgroep Voor Tertiaire En Kwartaire Geologie 16, 3–16.
Brand, U., Morrison, J.O. & Campbell, I.T. 1998: Strontium in sedimentary rocks. In: Geochemistry, 600–603. Encyclopedia of Earth Science. Springer. https://doi.org/10.1007/1-4020-4496-8_301
Calvert, S. E. & Pedersen, T.F. 2007: Elemental proxies for palaeoclimatic and palaeoceanographic variability in marine sediments: Interpretation and application. In: Hillaire–Marcel, C. & de Vernal, A. (eds): Developments in marine geology, vol. 1, Proxies in late cenozoic paleoceanography, 567–644. Elsevier. https://doi.org/10.1016/S1572-5480(07)01019-6
Chandra, A. P. & Gerson, A.R. 2010: The mechanisms of pyrite oxidation and leaching: A fundamental perspective. Surface Science Reports 65, 293–315. https://doi.org/10.1016/j.surfrep.2010.08.003.
Climate Foundation Skive 2025: Projekt C-ASH: CO_2-mineralisering med naturens teknologi i ny sammenhæng. Accessed October 2025. Available at: <https://www.klimafondenskive.dk/projekter/c-ash-co2-fiksering-med-naturens-teknologi-i-ny-sammenhaeng/>
Danielsen, M. & Thomsen, E. 1997: Palaeocene/Eocene diatomite in wells in the eastern North Sea. Aarhus Geoscience, Geology and Palaentology of the Mo-clay, no. 6, 19–24.
Dinesen, A., Michelsen, O. & Lieberkind, K. 1977: A survey of the Paleocene and Eocene deposits of Jylland and Fyn. Danmarks Geologiske Undersøgelse Serie B1, 15 pp. https://doi.org/10.34194/serieb.v1.7056
GEUS 1980: Borerapport - JUPITER – DGU nr. 46.611. https://data.geus.dk/JupiterWWW/borerapport.jsp?borid=32515
Gíslason, S.R., Sigurdardóttir, H., Aradóttir, E.S. & Oelkers, E.H. 2018: A brief history of CarbFix: Challenges and victories of the project's pilot phase. Energy procedia, carbon in natural and engineered processes: Selected contributions from the 2018 International Carbon Conference, vol. 146, 103–114. https://doi.org/10.1016/j.egypro.2018.07.014
Goldschmidt, V.M. 1937: The principles of distribution of chemical elements in minerals and rocks. The seventh Hugo Müller lecture, delivered before the Chemical Society on March 17th, 1937. Journal of the Chemical Society (Resumed), 655–673. https://doi.org/10.1039/JR9370000655
Gry, H. 1940: De istektoniske Forhold i Moleromraadet. Meddelelser fra Dansk Geologisk Forening 9, 586–627. https://2dgf.dk/xpdf/bull-1940-9-5-586-627.pdf
Güven, N. & Grim, R.E. 1978: Bentonites: Geology, mineralogy, properties and uses. Elsevier.
Hansen, M.U. 2018: Petrologisk og geokemisk beskrivelse af askelag i Harre borekernen, nordvest Jylland. Aarhus University [Unpublished master's thesis].
Heilmann-Clausen, C. 1995: Palæogene aflejringer over Danskekalken. Aarhus Geokompendier 1, 69–114.
Heilmann-Clausen, C., Nielsen, O. B. & Gersner, F. 1985: Lithostratigraphy and depositional environments in the Upper Paleocene and Eocene of Denmark. Bulletin of the Geological Society of Denmark 33, 287–323. https://doi.org/10.37570/bgsd-1984-33-26
Hrnjić, M., Hagen-Peter, G.A., Birch, T., Barfod, G.H., Sindbæk, S.M. & Lesher, C.E. 2020: Non-destructive identification of surface enrichment and trace element fractionation in ancient silver coins. Nuclear Instruments and Methods in Physics Research Section B: Beam Interactions with Materials and Atoms 478, 11–20. https://doi.org/10.1016/j.nimb.2020.05.019
Huggett, J. 1993: Petrology and diagenesis of Palaeogene clays from Ølst and Ålbækhoved, Denmark. Bulletin of the Geological Society of Denmark 40, 256–271. https://doi.org/10.37570/bgsd-1993-40-11
IPCC 2005: IPCC special report on carbon dioxide capture and storage. Prepared by Working Group III of the Intergovernmental Panel on Climate Change. Cambridge University Press.
IPCC 2018: Global warming of 1.5°C. An IPCC special report on the impacts of global warming of 1.5°C above pre-industrial levels and related global greenhouse gas emission pathways, in the context of strengthening the global response to the threat of climate change, sustainable development, and efforts to eradicate poverty. Cambridge University Press, 616 pp. https://doi.org/ 10.1017/9781009157940
IPCC 2023: Climate change 2023: Synthesis report. Contribution of Working Groups I, II and III to the Sixth Assessment Report of the Intergovernmental Panel on Climate Change. IPCC, Geneva, Switzerland, 184 pp. https://doi: 10.59327/IPCC/AR6-9789291691647
Jones, M.T. et al. 2019: Mercury anomalies across the Palaeocene–Eocene thermal maximum. Climate of the Past 15, 217–236. https://doi.org/10.5194/cp-15-217-2019
Jones, M.T. et al. 2023: Tracing North Atlantic volcanism and seaway connectivity across the Paleocene–Eocene thermal maximum (PETM). Climate of the Past 19, 1623–1652. https://doi.org/10.5194/cp-19-1623-2023
Kherif, F. & Latypova, A. 2020: Principal component analysis. In: Mechelli, A. & Vieira, S. (eds): Machine Learning. Academic Press. https://doi.org/10.1016/B978-0-12-815739-8.00012-2
Klimafonden Skive 2025: 'C-ASH: CO2-fiksering med naturens teknologi i ny sammenhæng'. Accessed 12 May 2025. https://www.klimafondenskive.dk/projekter/c-ash-co2-fiksering-med-naturens-teknologi-i-ny-sammenhaeng/
Knox, R.W.O'B. 1997: The Late Paleocene to Early Eocene ash layers of the Danish mo-clay (Fur Formation): Stratigraphic and tectonic significance. Aarhus Geoscience 6 (Geology and Paleontology of the Mo-Clay), 7–11.
Knox, R.W.O'B. et al. 2010: Cenozoic. In: Doornenbal, J.C. & Stevenson, A.G. (eds): Petroleum geological atlas of the southern Permian Basin area. EAGE Publications b.v. (Houten), 211–223.
Lackner, K.S., Wendt, C.H., Butt, D.P., Joyce, E.L. & Sharp, D.H. 1995: Carbon dioxide disposal in carbonate minerals. Energy 20, 1153–1170. https://doi.org/10.1016/0360-5442(95)00071-N
Lafargue, E., Marquis, F. & Pillot, D. 1998: Rock-Eval 6 applications in hydrocarbon exploration, production, and soil contamination studies. Revue de l'Institut Français Du Pétrole 53, 4. https://doi.org/10.2516/ogst:1998036

Larsen, L.M., Waagstein, R., Pedersen, A.K. & Storey, M. 1999: Trans-Atlantic correlation of the Palaeogene volcanic successions in the Faeroe Islands and East Greenland. Journal of the Geological Society 156, 1081–1095. https://doi.org/10.1144/gsjgs.156.6.1081

Larsen, L.M., Fitton, J.G. & Pedersen, A.K. 2003: Paleogene volcanic ash layers in the Danish Basin: Compositions and source areas in the North Atlantic Igneous Province. Lithos 71, 47–80. https://doi.org/10.1016/j.lithos.2003.07.001

Longman, J., Gernon, T.M., Palmer, M.R., Jones, M.T., Stokke, E.W. & Svensen, H.H. 2021: Marine diagenesis of tephra aided the Palaeocene-Eocene thermal maximum termination. Earth and Planetary Science Letters 571, 117101. https://doi.org/10.1016/j.epsl.2021.117101

MacLean, W. H. & Barrett, T.J. 1993: Lithogeochemical techniques using immobile elements. Journal of Geochemical Exploration 48, 109–133. https://doi.org/10.1016/0375-6742(93)90002-4

Michelsen, O., Thomsen, E., Danielsen, M., Heilmann-Clausen, C., Jordt, H. & Laursen, G.V. 1999: Cenozoic sequence stratigraphy in the eastern North Sea. In: de Graciansky, P.-C., Jacquin, T. & Vail, P.R. (eds): Mesozoic and Cenozoic sequence stratigraphy of European basins. SEPM Society for Sedimentary Geology 60. https://doi.org/10.2110/pec.98.02.0091

Morton, A.C. & Evans, J.A. 1988: Geochemistry of basaltic ash beds from the Fur Formation, island of Fur, Denmark. Bulletin of the Geological Society of Denmark 37, 1–9. https://doi.org/10.37570/bgsd-1988-37-01

Morton, A. C. & Knox, R.W.O'B. 1990: Geochemistry of Late Palaeocene and Early Eocene tephras from the North Sea Basin. Journal of the Geological Society 147, 425–437. https://doi.org/10.1144/gsjgs.147.3.0425

Moses, C.O. & Herman, J.S. 1991: Pyrite oxidation at circumneutral pH. Geochimica et Cosmochimica Acta 55, 471–482. https://doi.org/10.1016/0016-7037(91)90005-P

Nielsen, O.B. 1994a: Introduction to the Harre Borehole, Denmark. Aarhus Geoscience 1, 2–4.

Nielsen, O.B. 1994b: Lithostratigraphy and sedimentary petrography of the Paleocene and Eocene sediments from the Harre Borehole, Denmark. Aarhus Geoscience 1, 15–34.

Nielsen, O.B., Baumann, J., Zhang, D., Heilmann-Clausen, C. & Larsen, G. 1986: Tertiary deposits in Store Bælt. Geoskrifter Twentyfive Years of Geology in Aarhus 24, 235–253.

Nielsen, O.B., Friis, H. & Korsbech, U. 1994: Lithology and lithostratigraphy of the Harre Borehole, Denmark. Aarhus Geoscience 1, 5–14.

Orfanou, V., Birch, T., Lichtenberger, A., Rubina, R., Barfod, G.H., Lesher, C.E. & Eger, C. 2020: Copper-based metalwork in Roman to early Islamic Jerash (Jordan): Insights into production and recycling through alloy compositions and lead isotopes. Journal of Archaeological Science: Reports 33, 102519. https://doi.org/10.1016/j.jasrep.2020.102519

Orfanou, V., Birch, T., Sindbæk, S.M., Feveile, C., Barfod, G.H. & Lesher, C.E. 2021: On diverse arts: Crucible metallurgy and the polymetallic cycle at Scandinavia's earliest Viking town, Ribe (8th–9th c. CE), Denmark. Archaeological and Anthropological Sciences 13, 81. https://doi.org/10.1007/s12520-021-01308-1

Pedersen, A.K., Engell, J. & Rønsbo, J.G. 1975: Early Tertiary volcanism in the Skagerrak: New chemical evidence from ash-layers in the Mo-Clay of northern Denmark. Lithos 8, 255–268. https://doi.org/10.1016/0024-4937(75)90009-2

Pedersen, G.K. 1981: Anoxic events during sedimentation of a Palaeogene diatomite in Denmark. Sedimentology 28, 487–504. https://doi.org/10.1111/j.1365-3091.1981.tb01697.x

Pedersen, G.K. & Buchardt, B. 1996: The calcareous concretions (Cementsten) in the Fur Formation (Paleogene, Denmark): Isotopic evidence of early diagenetic growth. Bulletin of the Geological Society of Denmark 43, 78–86. https://doi.org/10.37570/bgsd-1996-43-09

Pedersen, G.K. & Surlyk, F. 1983: The Fur Formation, a Late Paleocene ash-bearing diatomite from northern Denmark. Bulletin of the Geological Society of Denmark 32, 43–65. https://doi.org/10.37570/bgsd-1983-32-03

Pedersen, G.K. et al. 2011: Moleområdets geologi – sedimenter, fossiler, askelag og glacialtektonik. Geologisk Tidsskrift 2011, 41–135.

Pedersen, S.A.S. 2008: Palaeogene diatomite deposits in Denmark: Geological investigations and applied aspects. GEUS Bulletin 15, 21–24. https://doi.org/10.34194/geusb.v15.5034

Ralph, J. *et al.* 2025: Gypsum. Mindat.org: The open access mineralogy database to accelerate data-intensive geoscience research. American Mineralogist 110, 833–844. https://doi:10.2138/am-2024-9486

Rimmer, S. 2004: Geochemical paleoredox indicators in Devonian–Mississippian black shales, central Appalachian Basin (USA). Chemical Geology 206, 373–91. https://doi.org/10.1016/j.chemgeo.2003.12.029

Roulet, M., Lucotte, M., Canuel, R., Farella, N., Courcelles, M., Guimarães, J.R.D., Mergler, D. & Amorim, M. 2000: Increase in mercury contamination recorded in lacustrine sediments following deforestation in the central Amazon. Chemical Geology 165, 243–266. https://doi.org/10.1016/S0009-2541(99)00172-2

Rudra, A., Petersen, H.I. & Sanei, H. 2024: Molecular characterization of biochar and the relation to carbon permanence. International Journal of Coal Geology 291, 104565. https://doi.org/10.1016/j.coal.2024.104565

Sanei, H., Goodarzi, F. & Flier-Keller, E.V.D. 2001: Historical variation of elements with respect to different geochemical fractions in recent sediments from Pigeon Lake, Alberta, Canada. Journal of Environmental Monitoring 3, 27–36. https://doi.org/10.1039/B006819P

Sanei, H., Grasby, S.E. & Beauchamp, B. 2015: Contaminants in marine sedimentary deposits from coal fly ash during the latest Permian Extinction. In: Blais, J.M., Rosen, M.R. & Smol, J.P. (eds): Environmental contaminants: Using natural archives to track sources and long-term trends of pollution. Springer. https://doi.org/10.1007/978-94-017-9541-8_5

Sanei, H., Ardakani, O.H., Akai, T., Akihisa, K., Jiang, C. & Wood, J.M. 2020: Core versus cuttings samples for geochemical and petrophysical analysis of unconventional reservoir rocks. Scientific Reports 10, 7920. https://doi.org/10.1038/s41598-020-64936-y

Schiøler, P. *et al.* 2007: Lithostratigraphy of the Palaeogene – Lower Neogene Succession of the Danish North Sea. Geological Survey of Denmark and Greenland Bulletin 12, 77 pp. https://doi.org/10.34194/geusb.v12.5249.

Schmitz, B. & Asaro, F. 1996: Iridium geochemistry of volcanic

ash layers from the early Eocene rifting of the northeastern North Atlantic and some other Phanerozoic events. Geological Sosiety of America Bulletin 108, 489–504. https://doi.org/10.1130/0016-7606(1996)108<0489:IGOVAL>2.3.CO;2

Schovsbo, N.H. & Petersen, H.I. 2024: Analysis of the applicability of cuttings samples to test seal integrity, examples from the Triassic to Jurassic interval in 8 wells in Eastern Denmark. Danmarks og Grønlands Geologiske Undersøgelse Rapport 2024/10, 67 pp. https://doi.org/10.22008/gpub/34731

Seifritz, W. 1990: CO2 disposal by means of silicates. Nature 345, 486–486. https://doi.org/10.1038/345486b0

Snæbjörnsdóttir, S.Ó., Oelkers, E.H., Mesfin, K., Aradóttir, E.S., Dideriksen, K., Gunnarsson, I., Gunnlaugsson, E., Matter, J.M., Stute, M. & Gislason, S.R. 2017: The chemistry and saturation states of subsurface fluids during the in situ mineralisation of CO2 and H2S at the CarbFix site in sw-Iceland. International Journal of Greenhouse Gas Control 58, 87–102. https://doi.org/10.1016/j.ijggc.2017.01.007

Snæbjörnsdóttir, S.Ó., Sigfússon, B., Marieni, C., Goldberg, D., Gislason, S.R. & Oelkers, E.H. 2020: Carbon dioxide storage through mineral carbonation. Nature Reviews Earth & Environment 1, 2. https://doi.org/10.1038/s43017-019-0011-8

Stokke, E.W., Liu, E.J. & Jones, M.T. 2020: Evidence of explosive hydromagmatic eruptions during the emplacement of the North Atlantic Igneous Province. Volcanica 3, 227–250. https://doi.org/10.30909/vol.03.02.227250

Stokke, E.W., Jones, M.T., Riber, L., Haflidason, H., Midtkandal, I., Schultz, B.P. & Svensen, H.H. 2021: Rapid and sustained environmental responses to global warming: The Paleocene–Eocene thermal maximum in the eastern North Sea. Climate of the Past 17, 1989–2013. https://doi.org/10.5194/cp-17-1989-2021

Stucki, J.W. 2013: Properties and behaviour of iron in clay minerals. In: Bergaya, F. & Lagaly, G. (eds): Developments in Clay Science 5, 559–611. Elsevier. https://doi.org/10.1016/B978-0-08-098258-8.00018-3

Taylor, S.R. & McLennan, S.M. 2003: Chemical composition and element distribution in the Earth's crust. In: Meyers, R.A. (Ed.): Encyclopedia of physical science and technology 697–719. Academic Press. https://doi.org/10.1016/B0-12-227410-5/00097-1

Thomsen, E. & Danielsen, M. 1995: Transitional Palaeocene-Eocene ash-bearing diatomite in the eastern North Sea. Tertiary Research 15, 111–120.

Torp, T.A. & Gale, J. 2004: Demonstrating storage of CO2 in geological reservoirs: The Sleipner and SACS projects. Energy, 6th International Conference on Greenhouse Gas Control Technologies 29, 1361–1369. https://doi.org/10.1016/j.energy.2004.03.104

Turekian, K.K. & Wedepohl, K.H. 1961: Distribution of the elements in some major units of the Earth's crust. Geological Society of America Bulletin 72, 175–192. https://doi.org/10.1130/0016-7606(1961)72[175:DOTEIS]2.0.CO;2

Winchester, J.A. & Floyd, P.A. 1977: Geochemical discrimination of different magma series and their differentiation products using immobile elements. Chemical Geology 20, 325–343. https://doi.org/10.1016/0009-2541(77)90057-2